

Generator Design for the Symphony Wave Power Device

by
Djurre Wikkerink

DELFT UNIVERSITY OF TECHNOLOGY

Generator Design for the Symphony Wave Power Device

by

Djurre Wikkerink

A thesis submitted in partial fulfillment for the
degree of Master of Science

in the
Faculty Electrical of Engineering, Mathematics and Computer Science
DC systems, Energy Conversion & Storage

August 2017

“Wind power kills all your birds. All your birds, killed. You know, the environmentalists never talk about that.”

Donald Trump, 2016

DELFT UNIVERSITY OF TECHNOLOGY

Abstract

Faculty Electrical of Engineering, Mathematics and Computer Science
DC systems, Energy Conversion & Storage

Master Thesis

by Djurre Wikkerink

Wave power is a large untapped source of renewable energy. There is a wide variety of wave energy converters and one of them is the Symphony Wave Power device. The aim of this thesis is to find the best generator design for the Symphony. There is some research available on generator designs for wave energy converters but the Symphony is a unique case, so a new research needed to be conducted.

Several generator types can be used in the Symphony. Compared to an induction and switched reluctance generator, the iron-cored permanent magnet synchronous generator (PMSG) seems a good choice because it is efficient and reliable. A disadvantage, however, is that, in the case of the Symphony, the iron losses are relatively high at partial loads. An air-cored PMSG does not have this problem since it has no iron losses at all. A drawback of the air-cored PMSG is that it needs more permanent magnetic material, which is expensive. Finally, it was decided to test and compare the iron-cored radial flux PMSG and the air-cored axial flux PMSG on both performance and costs.

For both generator types, an analytical model was built which puts out the efficiency and material cost. To find the best generator geometries for the case of the Symphony, an optimization procedure was created which minimizes both material costs and losses.

It was found that an axial flux air-cored PMSG is both cheaper and more efficient than a radial flux iron-cored PMSG. The iron losses of an iron-cored generator are relatively high at partial loads while the Symphony operates at partial loads most of the time.

Acknowledgements

I would like to thank Fred Gardner, Bauke Vriesema and Hans van Noorloos from Teamwork Technology in Alkmaar for the opportunity to do my research on the Symphony Wave Power device and for the weekly discussions and feedback.

From Delft University of Technology, I would like to thank Henk Polinder, Jianning Dong, and Faisal Wani for the realization of this research and for showing me the ropes in the world of electrical machinery.

Contents

Abstract	ii
Acknowledgements	iii
Symbols and Abbreviations	vii
1 Research Field	1
1.1 Wave Power	1
1.2 Types of Wave Power Devices	2
1.3 Symphony Wave Power Device	3
1.4 Research Objectives	4
1.5 Outline and Approach	5
2 Background	6
2.1 Literature Review	6
2.2 Generator Specification	7
2.2.1 Scope	7
2.2.2 Bounds	8
2.3 Proposed Generator Types	9
2.3.1 Induction Generators	9
2.3.2 Synchronous Generators	9
2.3.2.1 Iron-cored	9
2.3.2.2 Air-cored	10
2.3.3 Switched Reluctance Generators	11
2.4 Conclusion	12
3 Analytical Modelling	13
3.1 Methodology	13
3.1.1 Main Differences Air-cored and Iron-cored	14
3.1.2 Assumptions	14
3.1.3 Design Variables	14
3.2 Radial Flux Iron-cored Generator	15
3.2.1 Geometry	15
3.2.2 Magnetic Circuit and Induced Voltage	16
3.2.3 Losses and efficiency	19

3.2.3.1	Iron Losses	19
3.2.3.2	Copper Losses	20
3.2.4	Cost and Weight of the Materials	21
3.2.5	Torque Production	21
3.3	Axial Flux Air-cored Generator	22
3.3.1	Geometry	22
3.3.2	Windings	23
3.3.3	Magnetic Circuit and Induced Voltage	24
3.3.4	Losses and efficiency	26
3.3.4.1	Winding Eddy Currents	26
3.3.4.2	Copper Losses	27
3.3.5	Cost and Weight of the Materials	27
3.3.6	Torque Production	27
3.4	Conclusion	28
4	Thermal Model	29
4.1	Methodology	29
4.1.1	Conduction	30
4.1.2	Convection	31
4.1.3	Radiation	32
4.1.4	Thermal Network	32
4.1.5	Assumptions	33
4.2	Iron-cored Generator	33
4.2.1	Node Placement	33
4.2.2	Stator	34
4.2.3	Air Gap	35
4.2.4	Rotor	35
4.2.5	End Windings	36
4.3	Air-cored Generator	36
4.3.1	Node Placement	36
4.3.2	Stator	37
4.3.3	Air gap	37
4.3.4	Rotor	38
4.3.5	End Windings	39
5	Optimization	40
5.1	Optimization Variables and Constraints	40
5.2	Optimization Objective	41
5.3	Wave Spectrum Implementation	42
6	Results	43
6.1	Optimized Design	43
6.2	Results of the Analytical Model	44
6.3	Results of the Thermal Model	44
6.4	Losses and Costs	45
7	Conclusions and Recommendations	48
7.1	Conclusions	48

7.2 Recommendations and Further Research	49
A Wheater Conditions Leixous	55
B Used Numbers	56
C Thermal Models	58
C.1 Iron-Cored Generator	58
C.2 Air-Cored Generator	63
C.3 Thermal Resistances	66

Symbols and Abbreviations

A	surface area	m^2
AC	Alternating Current, Air-Cored	
\mathcal{A}	analytical model	
b_m	magnet width	m
b_s	slot width	m
b_t	tooth width	m
c	specific material cost	€kg^{-1}
C	costs, heat capacity, capacitance	$\text{€}, \text{JK}^{-1}, \text{F}$
D	air gap diameter	m
DC	Direct Current	
E	induced voltage	V
f	electrical frequency	Hz
F	radial conductivity factor	
g	air gap length, gravitational acceleration	m, ms^{-2}
G	electric conductance	S
h	heat transfer coefficient	$\text{Wm}^{-2}\text{K}^{-1}$
h_m	magnet height	m
h_{ry}	rotor yoke height	m
h_s	slot height	m
h_{sy}	stator yoke height	m
H_s	significant wave height	m
IC	Iron-cored	
I	current	A
J	current density	Am^{-2}
k	thermal conductance	$\text{W}^{-1}\text{K}^{-1}$
l_s	stator length	m
m	number of phases	
n	rotational speed	rpm
p	number of pole pairs	

P	power, thermal heat flow	W
PM	Permanent Magnet	
\mathcal{P}	permeance	H^{-1}
q	number of slots per pole per phase	
Q_s	number of stator slots	
R	thermal resistance, electric resistance	KW^{-1}, Ω
\mathcal{R}	reluctance	H
RMS	Root Mean Square	
SG	Synchronous Generator	
SRG	Switched Reluctance Generator	
T_e	wave period	s
T	torque	Nm
\mathcal{T}	thermal model	
U	voltage	V
ν	kinematic viscosity	m^2s^{-1}
WEC	Wave Energy Converter	
α	magnet width to pole pitch ratio	
β	tooth width to slot pitch ratio	
ε	emissivity	
η	machine efficiency	
θ_r	coil width angle	rad
Θ	temperature	K
λ	inner to outer diameter ratio	
μ	permeability	Hm^{-1}
ρ	resistivity, density	$\Omega\text{m}, \text{kgm}^{-3}$
σ	shear stress, Stephan-Boltzmann constant	$\text{Nm}^{-2}, \text{Wm}^{-2}\text{K}^4$
τ_p	pole pitch	m
τ_s	slot pitch	m
φ	phase angle	rad
Φ	magnetic flux	Wb
ψ	internal power angle	rad
ω	rational speed	rad s^{-1}

Chapter 1

Research Field

71% of the surface of our planet is covered by water which is constantly in motion. The oceans contain a huge, sometimes destructive, amount of energy. Due to the high energy density and predictability of waves, the ocean is a great potential source of renewable energy.

1.1 Wave Power

Ocean waves are created by the wind, which in its turn is created by solar energy. As solar energy is converted to wave energy, its intensity is concentrated from an annual average of 0.1-0.3 kW/m² horizontal surface of the earth to 2-3 kW/m in the area perpendicular to the direction of wave propagation. The high energy density and an estimated worldwide power potential of around 1 TW makes wave power a considerable source of energy [1]. The power per meter of wave front can be found using the following equation

$$P = \frac{1}{32\pi} \rho g^2 H^2 T \quad (1.1)$$

where ρ is the water density, g is the gravity acceleration, T is the wave period and H is the wave height. The wave height is defined as twice the amplitude. Ocean waves are a spectrum of multiple waves with different wave heights and period times. This spectrum is modelled using a statistical distribution of wave heights. In calculations, the significant wave height H_s is used, which is defined as the mean wave height of the highest one-third of the waves.

The rate at which a certain specific wave height annually occurs is again modelled by a statistical distribution. Measured data for this is also available, the occurency of waves near the coast of Portugal is shown in a scatter diagram found in appendix A.

The idea of wave power is not new, the first known patent was filed in 1799 [2]. During the oil crisis in the 1970s, the research in wave power was stimulated. Today's rising levels of greenhouse gases and climate change make wave power an important area of research again. Over the past centuries more than a thousand patents have been submitted for wave power [2], still, wave power is not yet applied on a large scale.

Some challenges arise when designing a wave energy converter (WEC). The ocean can be a hostile environment. Most of the time waves are in a normal state, but sometimes they can contain a destructive force which the device has to cope with. During a storm, survivability is a much more important issue than efficiency or even producing power at all. Also, the salty water of the ocean can cause corrosion, and maintenance should be kept to a minimum since offshore maintenance is expensive. Finally, finding investors is difficult since wave energy converters are not profitable yet.

1.2 Types of Wave Power Devices

Wave energy converters come in a large variety of sizes and shapes. Due to placement (shoreline, near-shore and offshore) and dependence on water depth, different approaches have been tested. At this moment around one hundred projects are at various stages of development [3]. Despite this large amount of projects, wave power devices can be categorized into three main categories: terminators, attenuators and point absorbers [4].

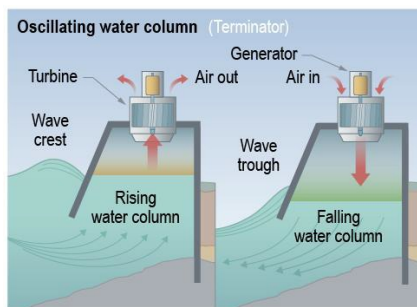


FIGURE 1.1: Terminator

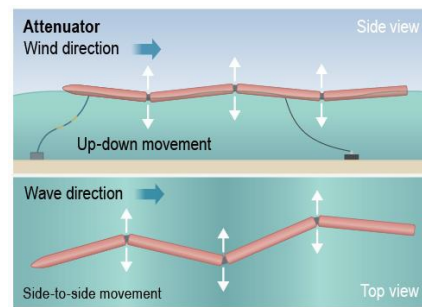


FIGURE 1.2: Attenuator

Terminators have their principle axis parallel to the wave front. An example of this is the Oscillating Water Column (OWC) shown in figure 1.1. As the water level rises, the pressure in the column builds up, forcing the excess air to drive a turbine. The main advantages of this design is its robustness. An OWC is placed on or near the shore

line and its chamber is made of concrete. Full-size prototypes have already been built around the world and their power capacity is in the range of 60-500 kW [3].

Attenuators lie parallel to the predominant wave direction as seen in figure 1.2. An example is the Pelamis. This 120-meter long device consists of four hollow steel floaters. The motion of the joints is resisted by rams pumping a high-pressure oil through a hydraulic motor. A set of three Pelamis WECs rated at 2.25 MW were installed in 2008, making it the worlds first grid connected wave farm [4].

Point absorbers (figure 1.3) are relatively small compared to the wavelength. Due to their size, the direction of the waves is not important. They can be floating on the surface like a buoy or submerged below sea level. An example of a point absorber is the Archimedes Wave Swing (AWS). The AWS converts the vertical motion of the device directly into electricity using a permanent magnet linear generator. One of the challenges is that the linear generator has to cope with attractive forces between the stator and translator [5]. The successor of the AWS is the Symphony Wave Power (SWP) device. This WEC is discussed in the following section.

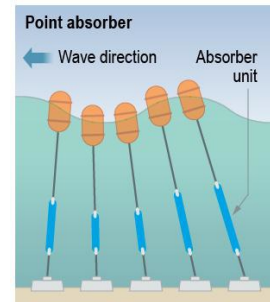


FIGURE 1.3: Pointabsorber

1.3 Symphony Wave Power Device

The Symphony is a submerged point absorber. It consists of a stationary part and a moving part. The top of the device is filled with air to create buoyancy. A schematic representation is shown in figure 1.4.

As the wave moves over the device, the hull gets pushed down by the water on top of it. A membrane filled with water slides down and decreases in volume. The contained water is forced out of the membrane through a turbine. The water leaving the turbine enters an air filled chamber causing the pressure in this chamber to increase. As the wave passes by and less water is on top of the device, both buoyancy and the pressure in the air chamber will bring the hull back to its original position. Water flows back from the air chamber through the turbine to the membrane.

The combination of the mass of the hull and the pressure in the air chamber can be seen as a mass spring system. By tuning the natural frequency of this system to be the same as the frequency of the incoming wave, the amplitude of the system will rise above the amplitude of the wave which is needed for optimal absorption of the wave power.

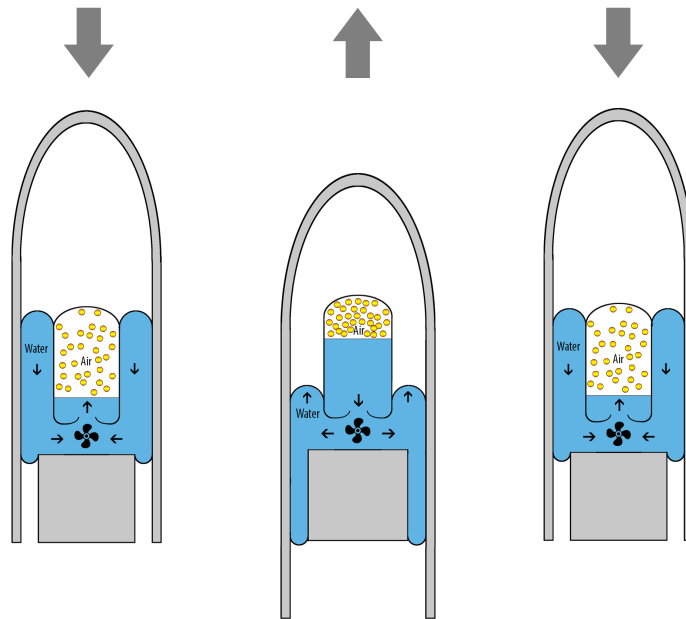


FIGURE 1.4: Operating principle of the Symphony

The Symphony converts its linear motion into a rotational motion via the turbine. There will be no attraction forces between the moving parts of the Symphony due to magnets. Another advantage is that the generator can operate at a relatively high rotational speed which will make the generator more compact and a lower torque rating is needed. The Symphony is still in a concept phase. A prototype will be built in the near future and deployed near the shore of Leixões in Portugal.

1.4 Research Objectives

This thesis focuses on designing the part of the Symphony which converts the mechanical power to electric power, the generator. The following research objectives have been defined.

- Find the best generator design for the Symphony Wave Power device.
 - What generator types are used in wave power?
 - What generator topologies are suitable for the Symphony?
 - What are the operating conditions for the generator of the Symphony?
 - What is the definition of “best”?

1.5 Outline and Approach

In chapter 2, a literature research is conducted. After that, the requirements for the generator are defined. Some conventional generator types are examined and finally, a generator type is chosen to be compared with a permanent magnet radial flux iron-cored synchronous generator.

Chapter 3 describes the design and analytical models for both the generators. These models will give a good estimate on efficiencies and costs of both generator types. In order to improve the accuracy of the analytical models, a thermal model for both generators was built. These models are discussed in chapter 4.

To ensure the most optimal design of the generators, an optimization procedure is needed. In chapter 5, this optimization procedure is discussed. In this chapter, an optimization objective is defined. This will be the criterion where the generators will be tested on.

With all the models in place, the generators can be tested. The results of the analytical model, the thermal model and the optimization are presented in chapter 6.

Finally, conclusions are drawn in chapter 7.

Chapter 2

Background

For the first prototype of the Symphony a generator was already chosen, an iron-cored radial flux permanent magnet synchronous generator (PMSG). In this thesis, the iron-cored radial flux PMSG will be used as a reference generator. Comparing other generator types with this generator should give a good insight in what generator design is best.

2.1 Literature Review

Traditionally, most of the electric power is generated by synchronous generators (SG) in fossil fueled power plants. Renewable energy sources don't share the same characteristics as fossil fuel. In wind power, for example, the use of variable speed generators can prevent large shock loads and improve the efficiency significantly [6] [7].

While some hydraulic pump and overtopping wave energy converters (WEC's) are designed for fixed-speed generators [8] [9], most WEC's, including the Symphony, operate with variable speeds and a low capacity factor (average-to-rated power ratio) [10] [11]. The low capacity factor causes the WEC to use an overrated generator under normal operating conditions. This increases costs and reduces the efficiency at partial loads.

The capacity factor and variable speed characteristics of the Symphony are similar to those of oscillating water columns (OWC) and direct drive WEC's. In [12], [13] and [14], induction generators are considered for OWC's. In [15] and [16] the use of a linear generator in direct drive WEC's is proposed. In [5], different generator types are tested to determine the best linear generator for a direct drive WEC. It has been concluded that, among the conventional generator types, a PMSG with iron in both stator is most suitable. The Symphony, however, operates at much lower speed than OWC's. It also uses a rotational generator, where direct drive WEC's use a linear generator.

2.2 Generator Specification

In the following sections, the functionality and requirements of the generator are defined. Also, the operating conditions are discussed.

2.2.1 Scope

As stated in section 1.3, the Symphony can be seen as a tuned mass spring system. To control the motion of the Symphony, a damper c is introduced as seen in figure 2.1. By compensating for the wave force, the damper force will ensure the moving hull to stay within its bounds. The excess energy is the energy the Symphony will deliver to the grid. The generator will undertake the task of the damper. Not only is the generator responsible for producing power, it is also functioning as a brake for the Symphony. It should, therefore, be operational at all times in order to prevent the Symphony to be out of control.

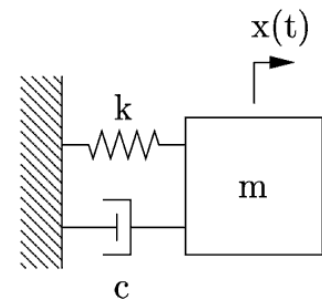


FIGURE 2.1: Schematic representation of the Symphony

The intensity of ocean waves differs from day to day. The blue line in Figure 2.2 shows the occurrence of wave spectra with a period time of $T_e = 10$ s. The red line represents the average power at the output of the turbine at this wave spectrum.

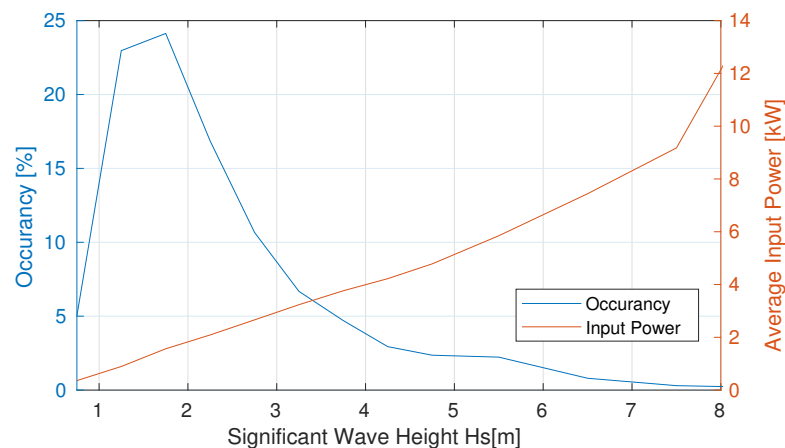


FIGURE 2.2: Occurance

It is clear that wave spectra with a specific wave height of $H_s = 1.5$ m are most occurring. Though the amount of power in higher waves is larger, they do not occur as frequently as lower waves. The highest sea state in which the Symphony should be in operation is at $H_s = 4.5$ m. This is where the first challenge in the design of a generator for

the Symphony lies. The generator should be efficient in the lower power range, while it should also be able to handle the higher power levels.

As stated in section 1.1, wave power is still not profitable yet. It is therefore important that all the components of the wave power device, including the generator, are as cheap as possible.

The Symphony is a submerged wave energy converter. This means it will be an expensive operation to perform maintenance on the machine. Therefore, the generator should have low maintenance.

2.2.2 Bounds

The turbine in the Symphony is connected to a shaft which drives the rotor of the generator. The rotational direction of the shaft changes twice wave period T_e . It is assumed that the ideal angular velocity is a sinusoidally shaped signal which is in phase with the torque on the shaft.

$$\omega = \hat{\omega} \sin\left(2\pi \frac{1}{T_e} t\right) \quad T = \hat{T} \sin\left(2\pi \frac{1}{T_e} t\right) \quad (2.1)$$

Since the mechanical power on the shaft is a product of angular velocity and torque, the power input for the generator is a sinusoid square shaped signal with a frequency of T_e^{-1} .

$$P = \omega T = \hat{\omega} \hat{T} \sin^2\left(2\pi \frac{1}{T_e} t\right) \quad (2.2)$$

The amount of power on the shaft is a result of wave height and wave period. The higher the waves, the more power that can be extracted. The Symphony is designed in such a way that this power level is only a consequence of torque. The peak value of the angular velocity $\hat{\omega}$ is not dependent on the wave height but is the same for every power level. The peak value for the rotational speed is at $\hat{n} = 350$ rpm.

The generator will be placed in a space with a relatively high radial to axial length ratio. This allows the generator to have a large air gap diameter.

2.3 Proposed Generator Types

To find the best generator type for the Symphony Wave Power device, most common generator types are examined in the following sections. The generator should have a high efficiency, low cost and since it is placed in the ocean, high reliability.

2.3.1 Induction Generators

Induction generators are known to be cheap and robust. The rotor of an induction generator moves slightly faster than the stator field which causes a changing magnetic field in the rotor to induce a current in the rotor bars. This current causes a magnetic field in the air gap. There are no brushes or magnets needed.

Usually, induction machines are efficient at high rotational speeds (1000-1500 rpm). The Symphony, however, operates at a much lower speed. This will make an induction machine less efficient. Also, induction machines have losses in the rotor bars which are not present with permanent magnet machines. Another disadvantage is that induction generators need the grid to start-up. The excitation current is drawn from the grid. Since the generator needs to start up twice every wave cycle this will be a problem. There are solutions for this, like using a capacitor bank [17].

2.3.2 Synchronous Generators

Synchronous generators do not share the same start-up problems as induction generators. The magnetic field is always there. The field can be excited by an excitation current through brushes or by permanent magnets. Since the generator needs to be of low maintenance, field excitation by slip rings is not desirable. The brushes wear out over time, so the magnetic field should be produced by permanent magnets. Though permanent magnets are expensive, the rotor field can be excited without any copper losses or wear. Both the iron-cored PMSG as the air-cored PMSG are examined in this section.

2.3.2.1 Iron-cored

Most of the synchronous generators are made out of iron. The stator consists of iron teeth where the copper windings are wound around. When the rotor field is rotating, the iron in the stator is constantly being magnetized and de-magnetized.

This causes both hysteresis losses and eddy current losses within the iron. The amount of losses in the stator iron is a function of air gap flux density and rotor speed. The air gap flux density is fixed due to the magnets. And since, for the Symphony, an increase in power only means an increase in torque rather than rotor speed, the iron losses will be constant over a range of power levels. To illustrate this, the efficiency of a PMSG with constant speed and a rated power of 20kW is shown in figure 2.3. At its rated power this machine has an efficiency of around 90%. In the lower power range, the efficiency drops drastically due to relative high iron losses. Since the Symphony should be able to capture the high power waves, but be efficient in the lower power range, this will cause a problem.



FIGURE 2.3: Efficiency of a 20kW PMSM

2.3.2.2 Air-cored

In an air-cored machine, the flux path is not routed through moving iron. Instead, the flux is produced by either one magnet, or two opposing magnets enclosing and moving around a stator coil. Since the copper in the coil has a low permeability, the reluctance between the magnets will be high. Figure 2.4 shows an example of an axial flux air-cored PMSG.

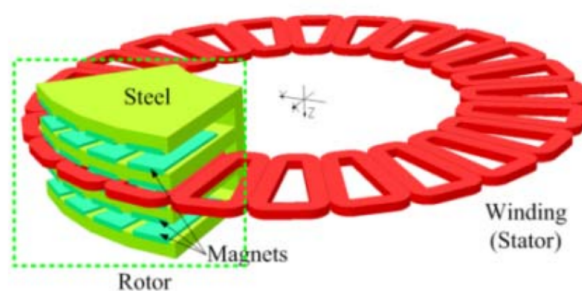


FIGURE 2.4: Air cored axial flux PMSG [18]

Since there is no varying magnetic field within the iron parts of this machine, there will be no iron losses. The iron loss problem described in section 2.3.2.1 is not present with an air cored machine, which is a big advantage. There are, however, eddy currents induced in the windings since the windings are directly exposed to the varying magnetic field.

With no iron in the stator, an air-cored machine is lighter than its iron-cored counterpart. This is an advantage because the Symphony would need less buoyancy and could, therefore, decrease its volume.

However, an air-cored machine has a relatively large air gap reluctance. There is no iron conducting the magnetic path. To compensate for this and create a sufficient magnet flux density, more permanent magnetic material is needed. This could increase the costs significantly

In [19], it is shown that an axial flux structure is an attractive solution when the axial length is typically shorter than the air gap diameter. If the length ratio is below 0.5, the overall volume of a radial flux structure is considerably higher than that of an axial flux structure. Since the Symphony has a relatively high diameter available, the axial flux machine would be a better choice.

2.3.3 Switched Reluctance Generators

The switched reluctance generator produces its field by separately exciting the stator coils. A schematic representation of an SRG is given in figure 2.5. When the rotor is aligned with an excited coil, the magnetic field tries to keep the rotor in this position. If the rotor is rotating, this creates a torque. By switching the excitation current from coil to coil in the opposite direction of the rotational direction, a torque is created at every rotor angle. The moment when a coil is activated is called the firing angle.

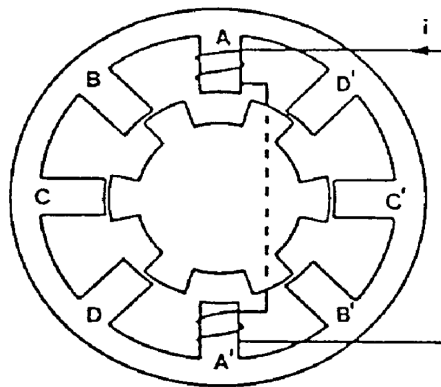


FIGURE 2.5: Switched Reluctance Machine

The switched reluctance generator (SRG) produces its field without the use of slip rings and magnets. This makes the machine cheaper than a PMSG and more reliable than a machine which needs an excitation current through slip rings.

Since the air gap field in an SRG is produced by an excitation current, the magnetic field strength is easily controllable. Depending on the input power, an optimum between

copper and iron losses can be found. This maximizes the output power for different input powers. The iron loss problem stated in section 2.3.2.1 is partially solved. However, both the stator as the rotor iron is exposed to a varying magnetic field. This will increase the amount of iron losses with respect to a PMSG. Also, the current which produces the magnetic field in the air gap causes extra copper losses. These losses are not present in a PMSG since its field is produced by magnets.

Because the torque in this machine is produced by pulses, there will be higher harmonic components in the torque waveform [20]. This will cause a significant torque ripple, which could damage the turbine and gears of the Symphony.

2.4 Conclusion

In this chapter, the functionality and requirements for the generator have been defined. Ultimately, the generator should comply with the following requirements.

1. The generator should be cheap.
2. The generator should be efficient.
3. The generator should have low maintenance.
4. The generator should have a high availability.

The iron-cored radial flux PMSG is selected as the designated generator, but the amount of iron losses are relatively high in lower sea states.

The axial flux air-cored variant could be a more efficient alternative since it has no iron losses. The amount of permanent magnetic material in an air-cored machine is higher, however, which increases costs. There is also an extra loss component, eddy currents in the windings.

The switched reluctance generator seems to be good a candidate as well. These machines are cheap because there are no permanent magnets. Also, the SRG is able to easily control the magnetic field strength in the air-gap so the generator can find an optimum between iron and copper losses. However, the SRG has a varying magnetic field in both the stator and the rotor iron which causes more iron losses than in a permanent magnet machine. Moreover, to excite the field an extra current is needed through the stator coils which means more losses.

The axial flux air-cored PMSG is chosen as an alternative for the radial flux iron-cored PMSG. Both machines will be modelled and compared in the following chapters to explore the best option.

Chapter 3

Analytical Modelling

As described in section 2.4, the goal is to compare an air-cored synchronous generator with an iron-cored synchronous generator on the basis of both efficiencies η and material costs C_{gen} . Two analytical models, \mathcal{A} , were developed of the form:

$$\eta, C_{gen} = \mathcal{A}(\mathbf{x}, P_{in}) \quad (3.1)$$

where \mathbf{x} is a vector containing the design variables and P_{in} is the input power. The following chapter describes how these models were built.

3.1 Methodology

There are many ways to model a generator [21]. In [22], [23], [24] and [25], an one-dimensional analytical model is used to model a generator. While the one-dimensional analytical model might not be the most accurate, it should provide a clear insight into the losses and costs of both machines. Another advantage is that it is easily incorporated into an optimization procedure.

Both generator types are modelled according to a one-dimensional analytical model. Based on the flux path produced by the magnets, an induced voltage can be calculated which is used to model the output power. The efficiency of the generators is calculated as the ratio of the output power over the known input power. The material costs are calculated using the machine's dimensions.

3.1.1 Main Differences Air-cored and Iron-cored

Since copper is a non-magnetic material, the air cored machine will have a higher air gap reluctance than the iron cored machine. It is expected that the leakage flux in the air cored machine will, therefore, be of more significance. This is taken into account and modelled in sections 3.2.2 and 3.3.3.

An air-cored machine will not have the magnetic flux routed through stator teeth. Instead, the flux density will vary within the stator coils. This will cause an extra loss component, eddy currents in the windings. This will be modelled in section 3.3.4.1.

The iron-cored machine is expected to have better cooling properties than the air-cored machine. This will have an effect on the stator resistance since it is a function of winding temperature. A thermal model is developed to test the impact of winding temperature on both machines. This model is discussed in chapter 4.

3.1.2 Assumptions

In order to simplify the models, the following assumptions are used in the models.

- The iron parts have infinite permeability. There is also no saturation of the iron.
- The flux, voltage and current waveforms are sinusoidal, which means there are no harmonics.
- The magnet and mechanical losses are negligible.

3.1.3 Design Variables

Both generators are modelled starting with a certain set of parameters. These are shown in table 3.1. With these variables as a starting point, the models can determine the geometries of the machines, and eventually, the efficiencies and material costs.

TABLE 3.1: Design parameters

Iron-cored (radial flux)	Symbol	Air-cored (axial flux)	Symbol
magnet width to pole pitch ratio	α	inner to outer diameter	λ
machine length	l_s	magnet width to pole pitch ratio	α
air gap diameter	D	outer diameter	D_o
slot height	h_s	slot height	h_s
number of poles	p	number of poles	p
magnet height	h_m	magnet height	h_m
stator yoke height	h_{sy}		
tooth width to slot pitch ratio	β		

In the optimization process, these parameters will be the optimization variables. By tuning the value of these variables, an optimized design can be achieved. This will be discussed in chapter 5.

3.2 Radial Flux Iron-cored Generator

The following section shows the design equations for the iron-cored generator.

3.2.1 Geometry

Figure 3.1 shows the used dimensions in the analytical model.

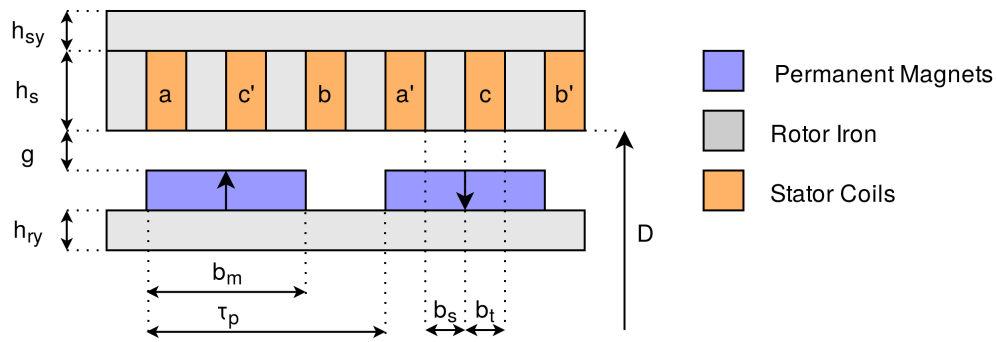


FIGURE 3.1: Dimensions of an iron-cored generator

From the air gap diameter D , we can start by finding the pole pitch τ_p , slot pitch τ_s .

$$\tau_p = \frac{\pi D}{2p} \quad (3.2)$$

$$\tau_s = \frac{\tau_p}{mq} \quad (3.3)$$

Since most power electronics are designed for a three phase system, the number of phases m is set to three. The number of slots per pole per phase q is chosen to be one. The air gap is set at 1mm. From the pole and slot pitch, the widths of the magnets, slots and teeth can be calculated.

$$b_m = \alpha \tau_p \quad (3.4)$$

$$b_s = (1 - \beta) \tau_s \quad (3.5)$$

$$b_t = \beta \tau_s \quad (3.6)$$

At this point, most of the machine's geometry is known. Only the height of the rotor yoke is still to be defined. This will depend on the flux density in the iron in order to prevent saturation.

This model uses a slotted stator. When the flux crosses the air gap, it will try to avoid the non-magnetic slots. In order to compensate for this slotting effect, an equivalent air gap length is used. The air gap length is multiplied by the Carter factor k_C .

$$g_{eff} = k_C g \quad (3.7)$$

There are several methods to calculate the Carter factor. The one used in this thesis is the original method proposed by Carter [26].

$$k_C = \frac{\tau_s}{\tau_s - \gamma g} \quad (3.8)$$

where τ_s is the slot pitch and γ is calculated as

$$\gamma = \frac{4}{\pi} \left[\frac{b_s}{2} \arctan \left(\frac{b_s}{2g} \right) - \ln \sqrt{1 + \left(\frac{b_s}{2g} \right)^2} \right] \quad (3.9)$$

3.2.2 Magnetic Circuit and Induced Voltage

The induced phase voltage can be found if the flux crossing the air gap is known. To estimate this value, a per pole equivalent circuit has been developed based on the different reluctances in the machine. With the remanence flux ϕ_r known, the air-gap flux ϕ_g can be calculated when the values of the reluctances are known. This circuit is shown in figure 3.2 and the method is based on the method found in [27] and [24].

The iron parts are assumed to have an infinite permeability, so stator reluctance \mathcal{R}_s and rotor reluctance \mathcal{R}_r are set to zero. The magnet-to-magnet and magnet-to-rotor reluctances are modelled by \mathcal{R}_{mm} and \mathcal{R}_{mr} respectively.

The air-gap reluctance is calculated as follows

$$\mathcal{R}_g = \frac{g_{eff}}{\mu_0 (b_m + 2g_{eff}) l_s} \quad (3.10)$$

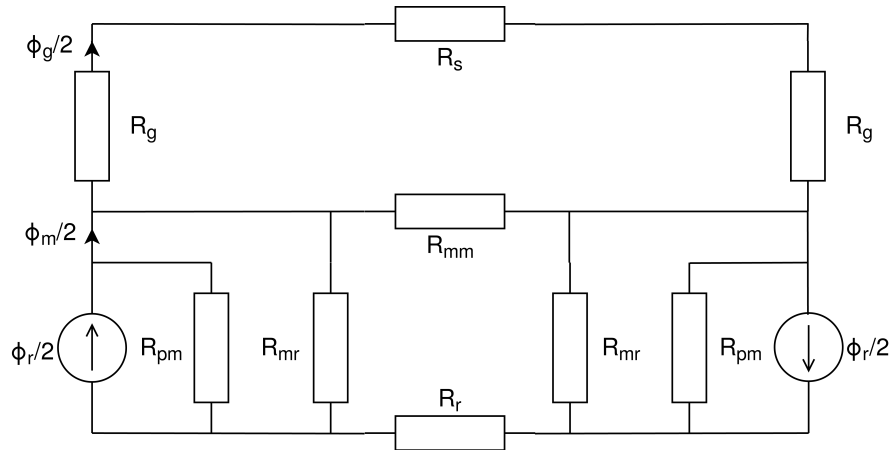


FIGURE 3.2: Flux path

where the $2g_{eff}$ term in the denominator is present to consider the fringing effect.

The permanent magnet reluctance can be found in a similar way

$$\mathcal{R}_{pm} = \frac{h_m}{\mu_0 \mu_{rm} b_m l_s} \quad (3.11)$$

To find the magnet-to-rotor and magnet-to-magnet reluctance, the circular-arc straight-line permeance model is used based on the model found in [27]. The flux path from the magnet-to-rotor and from the magnet-to-magnet are shown yellow in figure 3.3.

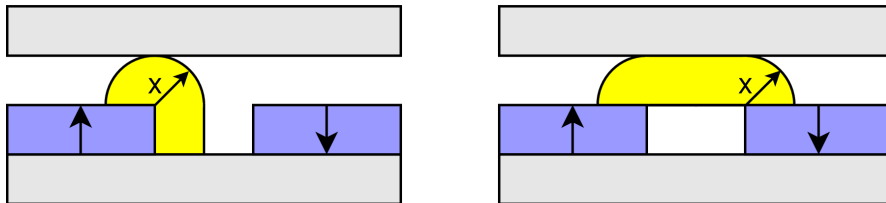


FIGURE 3.3: Magnet-to-rotor and magnet-to-magnet leakage flux

The permeances can be found by summing up the permeance lengths where x runs from 0 to g_{eff} as follows

$$\mathcal{P}_{mr} = \mu_0 l_s \int_0^{g_{eff}} \frac{1}{h_m + \pi x} dx \quad \mathcal{P}_{mm} = \mu_0 l_s \int_0^{g_{eff}} \frac{1}{\tau_p - b_m + \pi x} dx \quad (3.12)$$

By solving these integrals, the magnet-to-magnet and magnet-to-rotor permeance can be calculated.

$$\mathcal{P}_{mr} = \frac{\mu_0 l_s}{\pi} \ln \left(1 + \frac{\pi g_{eff}}{h_m} \right) \quad \mathcal{P}_{mm} = \frac{\mu_0 l_s}{\pi} \ln \left(1 + \frac{\pi g_{eff}}{\tau_p - b_m} \right) \quad (3.13)$$

The magnet-to-magnet permeance equation only holds when $g_{eff} < \frac{\tau_p - b_m}{2}$, which is the case in this model. From here the magnet-to-rotor and magnet-to-magnet reluctances are easily calculated

$$\mathcal{R}_{mr} = \frac{1}{\mathcal{P}_{mr}} \quad \mathcal{R}_{mm} = \frac{1}{\mathcal{P}_{mm}} \quad (3.14)$$

At this point, all the reluctances are known. The circuit in figure 3.2 can be simplified to an equivalent circuit shown in figure 3.4.

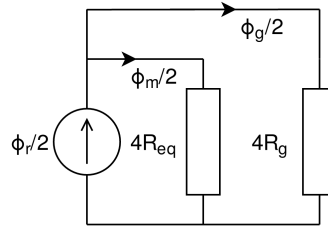


FIGURE 3.4: Equivalent circuit

The equivalent reluctance \mathcal{R}_{eq} for \mathcal{R}_{pm} , \mathcal{R}_{mr} and \mathcal{R}_{mm} is calculated as:

$$\mathcal{R}_{eq} = \frac{\mathcal{R}_{pm}}{1 + 2\frac{\mathcal{R}_{pm}}{\mathcal{R}_{mr}} + 4\frac{\mathcal{R}_{pm}}{\mathcal{R}_{mm}}} \quad (3.15)$$

The remanence flux Φ_r depends on both the size of the magnets as the strength of the magnetic material.

$$\Phi_r = B_r b_m l_s \quad (3.16)$$

With all the reluctance values and the remanence flux known, finally, the air gap flux Φ_g can be calculated.

$$\Phi_g = \frac{1}{1 + \frac{\mathcal{R}_g}{\mathcal{R}_{eq}}} \Phi_r \quad (3.17)$$

The peak of the flux density in the air gap, \hat{B}_g , depends on the surface area of the air gap of one pole.

$$\hat{B}_g = \frac{\Phi_g}{l_s \tau_p} \quad (3.18)$$

In this case, the flux crossing the air gap is a rectangular shaped signal. Since it is assumed that the waveforms are sinusoidal, we are only interested in the fundamental frequency which is found as follows

$$\hat{B}_{g1} = \hat{B}_g \frac{4}{\pi} \sin\left(\alpha \frac{\pi}{2}\right) \quad (3.19)$$

Finally, the induced voltage can be calculated. The induced RMS voltage is proportional to both frequency and air gap flux density.

$$E = k_w N 2\pi f \frac{1}{\sqrt{2}} \hat{B}_{g1} \frac{l_s D}{p} \quad (3.20)$$

where N represents the number of windings per phase and k_w is the winding factor. Since this machine has single-layer full-pitch non-skewed integer-slot windings, k_w is equal to 1.

3.2.3 Losses and efficiency

The efficiency η of a generator is defined as the ratio between input and output power.

$$\eta = \frac{P_{out}}{P_{in}} = \frac{P_{in} - P_{Fe} - P_{Cu}}{P_{in}} \quad (3.21)$$

where P_{Fe} and P_{Cu} are the iron and copper losses respectively which will be discussed in the following sections.

3.2.3.1 Iron Losses

The iron losses in this model consist of hysteresis losses and eddy current losses in the stator iron. The amount of loss can be estimated using the data provided by the manufacturer of the iron laminations. The manufacturer measured the core and eddy current losses of his lamination with a flux density of 1.5 T at a frequency 50 Hz. Using the values $P_{0(hy)}$ and $P_{0(ed)}$, the amount of iron losses in our own machine can be found.

$$P_{hy} = k_{hy} m_{Fe} \left(\frac{\hat{B}_{Fe}}{1.5} \right)^{1.6} \left(\frac{f}{50} \right) P_{0(hy)} \quad (3.22)$$

$$P_{ed} = k_{ed} m_{Fe} \left(\frac{\hat{B}_{Fe}}{1.5} \right)^2 \left(\frac{f}{50} \right)^2 P_{0(ed)} \quad (3.23)$$

where m_{fe} is the mass of the iron and \hat{B}_{Fe} the magnetic flux density within this iron. The factors k_{hy} and k_{ed} are empirical loss factors. These factors are here to compensate for the difference between test conditions and the conditions in a real machine. Both P_0 as k have different values for stator teeth and stator yoke. The values for these factors are given in Appendix B

3.2.3.2 Copper Losses

The copper losses of the machine are found using Joule's law

$$P_{Cu} = 3I_s^2 R_s \quad (3.24)$$

The per phase resistance of the windings can be found using Pouillet's law

$$R_s = \rho_{Cu} \frac{l N_s}{A_s k_f} \quad (3.25)$$

where l is the length of the wire, N_s is the number of conductors per slot, A_s the area of a slot and ρ_{Cu} the electrical resistivity of copper. Ideally, the entire slot area should be filled with copper. The wire, however, is shaped round and contains an insulation. To compensate for this, fill factor k_f is introduced. The resistivity of copper is depended on its temperature according to the following formula

$$\rho_{Cu} = \rho_{Cu(20^\circ C)} (1 + \Delta\Theta \alpha_{Cu}) \quad (3.26)$$

where $\rho_{Cu(20^\circ C)}$ is the resistivity of copper at 20°C and α_{Cu} is the temperature coefficient of copper. To find the value for temperature difference $\Delta\Theta$ at a given input power, a thermal model is developed which is presented in chapter 4.

With R_s known, we only have to determine the stator current I_s . Since we only know the mechanical input power, I_s can be found solving the following quadratic expression

$$0 = 3R_s I_s^2 + 3E I_s \cos \psi + P_{Fe} - P_{in} \quad (3.27)$$

where ψ is the internal power angle which is assumed to be 90 degrees. The iron losses are already determined in the previous section, they are not proportional to the stator current.

3.2.4 Cost and Weight of the Materials

When calculating the costs of this machine, only the active material costs are considered. The costs of the materials are found by multiplying the mass with its specific cost.

$$C_{gen} = c_{Fe}m_{Fe} + c_{Cu}m_{Cu} + c_{pm}m_{pm} \quad (3.28)$$

The values of the specific costs c_{Fe} , c_{Cu} and c_{pm} are given in appendix B. The masses can be found by multiplying the materials volumes with their mass density.

3.2.5 Torque Production

The generator should be able to deliver a minimum amount of torque whilst not exceeding the maximum winding temperature.

The temperature of the windings will be dependent on the maximum current through the windings, the geometry and the cooling of the windings. The value for the maximum allowable RMS phase current, I_{max} , will be determined in the thermal model described in chapter 4. From this the maximum electric loading A_{max} can be found [23].

$$A_{max} = \frac{N_s I_{max}}{\tau_s} \quad (3.29)$$

where N_s is the number conductors in a slot. The shear stress σ on the rotor can be found by multiplying the electric loading with the RMS value of the magnetic loading \hat{B}_{g1}

$$\sigma_{max} = \frac{1}{\sqrt{2}} \hat{B}_{g1} A_{max} \quad (3.30)$$

Finally, the maximum torque the machine is able to deliver T_{max} is found by multiplying the shear stress σ with the rotor area and the lever arm

$$T_{max} = \sigma_{max} \pi D l_s \frac{D}{2} \quad (3.31)$$

It should be noted that the maximum torque that the machine is able to produce is proportional to the volume of the rotor.

3.3 Axial Flux Air-cored Generator

The air-cored generator has some differences with respect to the iron cored generator. The flux is routed in the axial direction which has some consequences for the determination of the geometry.

3.3.1 Geometry

The geometry of the air-cored machine is shown in figure 3.5.

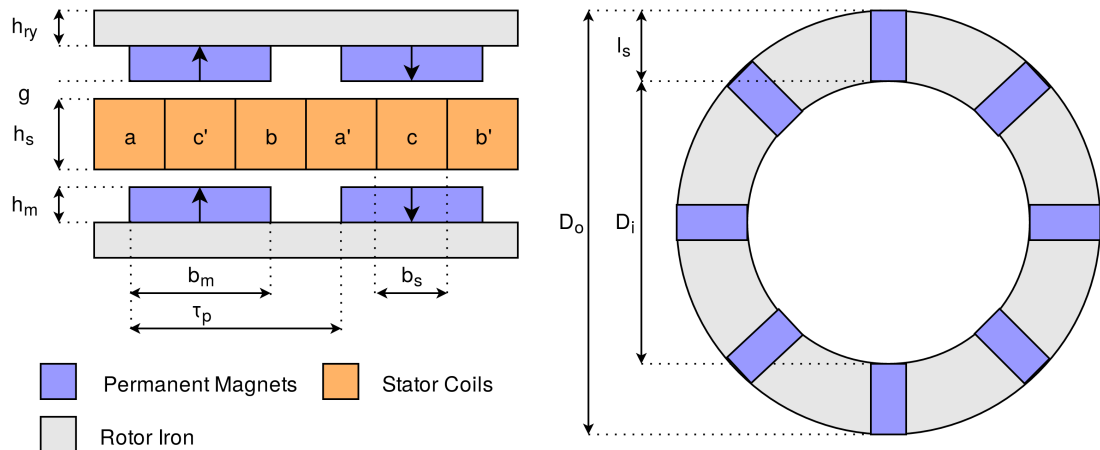


FIGURE 3.5: Dimensions of an air-cored generator

The magnets have a rectangular shape. This shape is chosen so the flux density is evenly distributed within the rotor yoke as shown in [19].

With the outer diameter of the machine as a starting point, the inner diameter is calculated using the known ratio λ of the two. From there the stator length is calculated.

$$D_i = \lambda D_o \quad (3.32)$$

$$l_s = \frac{1}{2}(1 - \lambda)D_o \quad (3.33)$$

The modelling of an axial flux machine differs from the modelling of a radial flux machine. The pole pitch is not constant as the radius increases. In [28] a layered model is

used where the machine is divided into small layers with each their own pole pitch. In this model, the pole pitch in between D_i and D_o is taken as the mean pole pitch τ_{ph} . The inner pole pitch τ_i and outer pole pitch τ_o are used as well.

$$\tau_{pi} = \frac{\pi D_i}{2p} \quad \tau_{ph} = \frac{\pi(D_o + D_i)}{4p} \quad \tau_{po} = \frac{\pi D_o}{2p} \quad (3.34)$$

The inner pole pitch is used to find the magnet width and the slot width

$$b_m = \alpha \tau_{pi} \quad (3.35)$$

Slot width b_s is equal to the slot pitch τ_s , there are no stator teeth in between.

$$b_s = \tau_s = \frac{\tau_{pi}}{mq} \quad (3.36)$$

The available space for the windings varies with the radius. The inner pole pitch, τ_{pi} , is taken into account to calculate the slot width, however.

3.3.2 Windings

To optimally make use of the space in the stator, the winding segmentation in figure 3.6 is used.

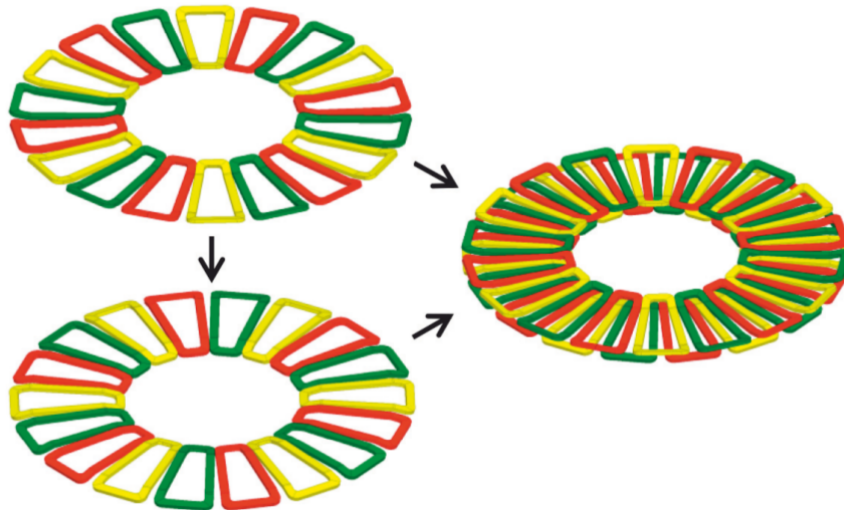


FIGURE 3.6: Winding segmentation AC PMSM [31]

The length of the copper wires is calculated according to the following formula

$$l_{Cu} = pN_s \left(2l_s + \tau_{pi} + \tau_{po} + 4 \frac{h_s}{2\sin(\frac{\pi}{6})} \right) \quad (3.37)$$

3.3.3 Magnetic Circuit and Induced Voltage

Since the air cored generator has a relatively large air gap, the leakage flux will have a large impact on the flux density crossing the air gap. The following model follows the same approach as presented in section 3.2.2. Figure 3.7 shows the equivalent reluctance schematic.

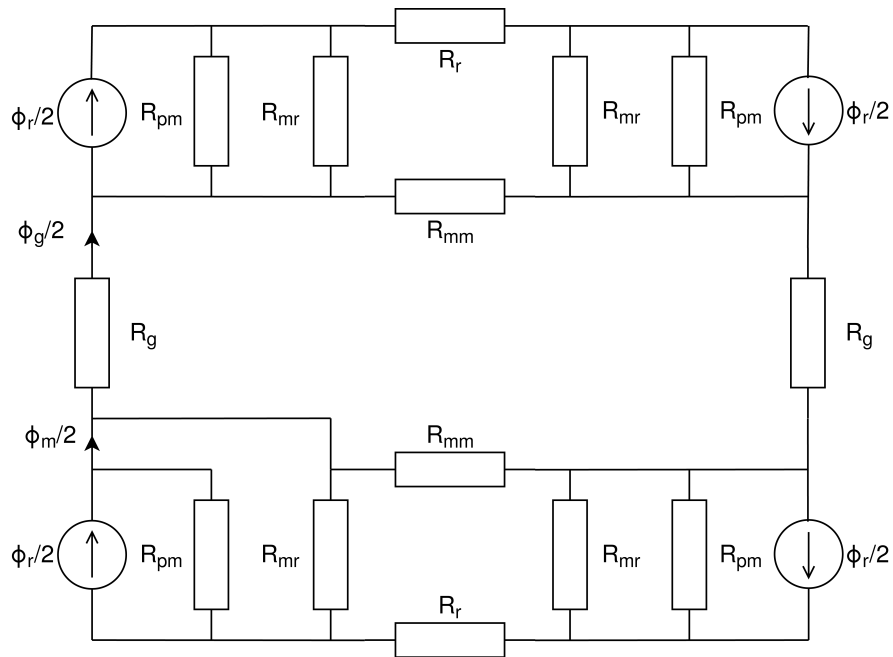


FIGURE 3.7: Flux path

Air gap reluctance \mathcal{R}_g is found using the sum of the stator height h_s and twice the air gap length $2g$.

$$\mathcal{R}_g = \frac{h_s + 2g}{\mu_0 \tau_p h l_s} \quad (3.38)$$

The reluctance of the magnets \mathcal{R}_{pm} is found in a similar way.

$$\mathcal{R}_{pm} = \frac{h_m}{\mu_0 \mu_{rm} b_m l_s} \quad (3.39)$$

Using the circular-arc straight-line permeance model, the magnet-to-rotor permeance \mathcal{P}_{mr} and magnet-to-magnet permeance \mathcal{P}_{mm} can be found.

$$\mathcal{P}_{mr} = \frac{\mu_0 l_s}{\pi} \ln \left(1 + \frac{\pi \frac{\tau_{ph} - b_m}{2}}{h_m} \right) \quad \mathcal{P}_{mm} = \frac{\mu_0 l_s}{\pi} \ln \left(1 + \pi \frac{g + \frac{h_s}{2}}{\tau_{ph} - b_m} \right) \quad (3.40)$$

In this equations, the mean pole pitch τ_{ph} is used.

With all the reluctances known, the circuit from 3.7 can be simplified to an equivalent circuit shown in 3.8. The equivalent reluctance \mathcal{R}_{eq} is calculated as follows:

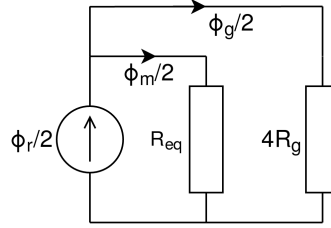


FIGURE 3.8: Equivalent circuit

$$\mathcal{R}_{eq} = \frac{8\mathcal{R}_{pm}}{1 + 2\frac{\mathcal{R}_{pm}}{\mathcal{R}_{mr}} + 4\frac{\mathcal{R}_{pm}}{\mathcal{R}_{mm}}} \quad (3.41)$$

The flux crossing the air gap can now be calculated.

$$\Phi_g = \frac{1}{1 + \frac{4\mathcal{R}_g}{\mathcal{R}_{eq}}} B_r b_m l_s \quad (3.42)$$

The peak of the flux density in the air gap, \hat{B}_g , depends on the surface area of the air gap of one pole.

$$\hat{B}_g = \frac{\Phi_g}{l_s \tau_{ph}} \quad (3.43)$$

In this case, the flux crossing the air gap is a rectangular shaped signal. The sinusoidal fundamental frequency is found as follows

$$\hat{B}_{g1} = \hat{B}_g \frac{4}{\pi} \sin(\alpha \frac{\pi}{2}) \quad (3.44)$$

Finally, the induced voltage is found.

$$E = k_w N 2\pi f \frac{1}{\sqrt{2}} \hat{B}_{g1} \frac{l_s (D_o + D_i)}{2p} \quad (3.45)$$

The winding factor k_w for the air-cored machine is different than the winding factor for an iron-cored machine because the flux is not concentrated in iron teeth anymore. to compensate for this the new winding factor is calculated as follows.

$$k_w = k_d k_p \quad (3.46)$$

where distribution factor k_d is one because the number of slot per pole per phase is one. The pitch factor k_p is calculated using the following equation [29]

$$k_p = \frac{2 \sin(\frac{\theta_r}{2})}{\theta_r} \quad (3.47)$$

where θ_r is the coil width angle at the average radius of the machine.

3.3.4 Losses and efficiency

The efficiency η of the air-cored generator is calculated as follows

$$\eta = \frac{P_{out}}{P_{in}} = \frac{P_{in} - P_{ed} - P_{Cu}}{P_{in}} \quad (3.48)$$

One of the advantages of using an air-cored machine is that there are no iron losses in the stator. There will be eddy current losses in the stator windings, however. These are represented by P_{ed} . The eddy current losses and the copper losses P_{Cu} are discussed in the following sections.

3.3.4.1 Winding Eddy Currents

Where in an iron-cored machine most of the flux is routed through the stator teeth, the flux in an air-cored passes through the stator coils. This causes a varying magnetic field within the windings which will cause a current. Due to the resistivity of the windings, the currents will cause power to be dissipated. These winding eddy currents are expected to be of significance and therefore modelled according to the following standard formula.

$$P_{ed} = m \frac{\pi l d^4 \hat{B}_{g1}^2 \omega^2}{32 \rho_{Cu}} \quad (3.49)$$

where m is the number of phases, l the length and d the diameter of the wire of the phases. It should be noted that the eddy current losses in the windings are proportional

to d^4 . Using thin parallel conductors will decrease the winding eddy current losses drastically. A disadvantage of using multiple parallel wires is that it reduces the filling factor. Another problem of using parallel wires is that there may be circulating currents between these wires, which cause circulating eddy current losses. This problem can be solved by twisting the parallel conductors [32].

The use of equation 3.49 has the advantage that it can be easily incorporated in the optimization procedure. It is proven in [30] however, that the use of a more complicated model will improve the accuracy significantly. This model assumes sinusoidal flux waveforms. In reality, the flux waveforms contain higher harmonic components. Since the eddy current losses are proportional to ω^2 , the higher harmonics will have a significant impact on the amount of losses.

3.3.4.2 Copper Losses

The copper losses in this model are found in the same way as described in section 3.2.3.2. The only difference is in finding stator resistance R_s .

$$R_s = \rho_{Cu} \frac{l_{Cu} N_s}{A_s k_f} \quad (3.50)$$

The fill factor k_f is a different value to compensate for the epoxy casting in the stator. The value for k_f is given in appendix B.

3.3.5 Cost and Weight of the Materials

The air-cored machine has one extra cost item with respect to the iron-cored machine. The epoxy in the stator is taken into account as well.

$$C_{gen} = c_{Fe} m_{Fe} + c_{Cu} m_{Cu} + c_{pm} m_{pm} + c_{ep} m_{ep} \quad (3.51)$$

The value for the specific cost of epoxy can be found in appendix B.

3.3.6 Torque Production

The maximum torque the air-cored machine will be able to produce is calculated using the same method as with the iron-cored machine in section 3.2.5.

$$T_{max} = \sigma_{max} \pi \left[\left(\frac{D_o}{2} \right)^2 - \left(\frac{D_i}{2} \right)^2 \right] \frac{D_o + D_i}{4} \quad (3.52)$$

where the surface of the rotor annulus is taken as the air gap area, and the center between the outer and inner radius as the lever arm. The shear stress σ_{max} is found by using equation 3.30. This equation also applies for axial flux machines.

3.4 Conclusion

For both the iron-cored as the air-cored generator, an analytical model was developed. Some assumptions were made in order to simplify the models. A simple model can be implemented in the optimization procedure more easily regarding computing time. The assumptions cause the models to be more inaccurate though, but still, they should provide a good estimation of efficiency and costs of both the radial flux iron-cored and the axial flux air-cored permanent magnet synchronous generators.

Chapter 4

Thermal Model

As described in sections 3.2.3 and 3.3.4, the temperature in the windings Θ_w should be known to ensure the machine does not exceed the maximum temperature of the designated insulation class limit. Two thermal models \mathcal{T} were developed of the form:

$$\Theta_w = \mathcal{T}(\mathbf{x}, \mathbf{P}_{loss}) \quad (4.1)$$

where \mathbf{x} is a vector containing the design variables and \mathbf{P}_{loss} is a vector containing all the loss components or heat sources in the machine. The following chapter describes how these models were built.

4.1 Methodology

The temperatures in the windings can be found by using a thermal model. Usually, a lumped parameter model is used for this. In [33] and [34], the thermal model of a radial flux machine is discussed. In [35] and [36], the thermal model of an axial flux machine is discussed. In [37], the difference in air-gap convection between radial and axial flux machines are discussed.

To find the temperatures and heat flow in the generators, a thermal equivalent circuit is used. The thermal domain is analogous to the electric domain according to table 4.1 [23].

TABLE 4.1: Thermal and electric analogy

Thermal domain	Symbol	Unit	Electric domain	Symbol	Unit
Quantity of heat	Q	J	Charge	Q	C
Heat flow	P	W	Current	I	A
Temperature	Θ	K	Voltage	U	V
Resistance	R	KW^{-1}	Resistance	R	Ω, VA^{-1}
Conductance	K	WK^{-1}	Conductance	G	S, AV^{-1}
Heat capacity	C	JK^{-1}	Capacitance	C	F, CV^{-1}
Conductivity	k	$\text{WK}^{-1}\text{m}^{-1}$	Conductivity	σ	Sm^{-1}

4.1.1 Conduction

Thermal conduction is the transfer of heat due to the movement of particles within a body. The thermal resistance of a body can be found using the following equation.

$$R = \frac{L}{kA} \quad (4.2)$$

Here, L is the length of the body parallel to the heat flow path, k the thermal conductivity of the material and A the area perpendicular to the heat flow path.

In [33], an induction machine is modelled using general cylindrical components. Since the parts of the machines in this thesis are cylindrical, this technique is used here as well. Figure 4.1 shows the temperatures at the four surfaces of a hollow cylinder with outer radius r_1 and inner radius r_2 . The heat flows are separated in axial and a radial heat flow. The thermal resistances are shown in figure 4.2 where resistances with suffix a are the axial resistances and with suffix r the radial resistances. Θ_m is the mean temperature of the cylinder and U is the heat source.

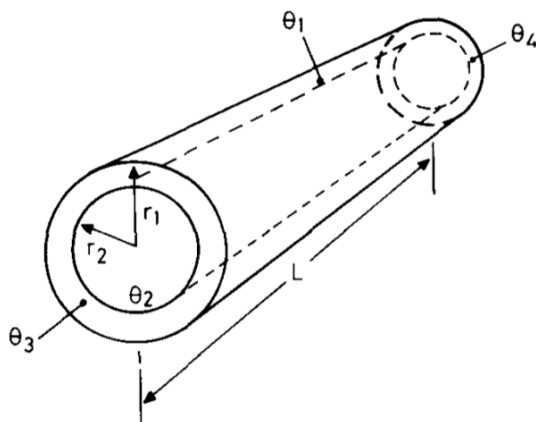


FIGURE 4.1: Cylindrical component [33]

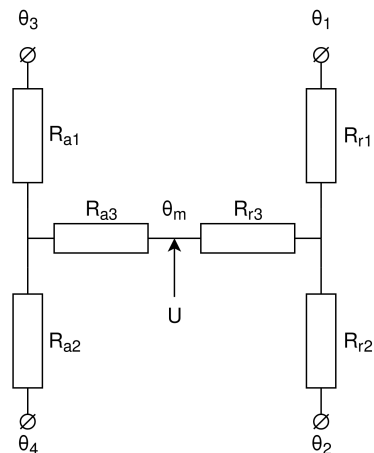


FIGURE 4.2: Resistance network

With some geometrical manipulations, equation 4.2 can be rewritten for the cylinders axial and radial directions as follows

$$R_{1a} = R_{2a} = \frac{L}{2\pi k_a(r_1^2 - r_2^2)} \quad (4.3)$$

$$R_{1r} = \frac{1}{4\pi k_r L} \left[1 - \frac{2r_2^2 \ln\left(\frac{r_1}{r_2}\right)}{r_1^2 - r_2^2} \right] \quad (4.4)$$

$$R_{1r} = \frac{1}{4\pi k_r L} \left[1 - \frac{2r_2^2 \ln\left(\frac{r_1}{r_2}\right)}{r_1^2 - r_2^2} \right] \quad (4.5)$$

Thermal resistances R_{3a} and R_{3r} are the interconnecting resistances which are calculated as follows.

$$R_{3a} = \frac{-L}{6\pi k_a(r_1^2 - r_2^2)} \quad (4.6)$$

$$R_{r3} = \frac{-1}{8\pi(r_1^2 - r_2^2)k_r L} \left[r_1^2 + r_2^2 - \frac{4r_1^2 r_2^2 \ln\left(\frac{r_1}{r_2}\right)}{r_1^2 - r_2^2} \right] \quad (4.7)$$

The iron-cored generator is symmetrical in the axial direction. This means $\Theta_3 = \Theta_4$. With this property, only half of the machine needs to be modelled. In this case, the resistances are multiplied by a factor 2 and the axial resistances can be modelled by an equivalent resistance R_{eq} .

$$R_{eq} = 2(R_{3a} + R_{1a} \setminus R_{2a}) \quad (4.8)$$

4.1.2 Convection

Convection is the transfer of heat due to the movement of fluids. The thermal resistance for convection from a solid to a fluid is found as follows

$$R = \frac{1}{h_c A} \quad (4.9)$$

where h_c is the convection heat transfer coefficient and A is the surface area of the solid in contact with the fluid. The determination of the convection heat transfer coefficients will be discussed in the modelling sections 4.2 and 4.3.

4.1.3 Radiation

Radiative heat transfer is a form of heat transfer due to electromagnetic radiation. The thermal resistance for radiation is found as follows

$$R = \frac{1}{h_r A} \quad (4.10)$$

Here h_r is the radiative heat transfer coefficient and A is the surface area of the solid. The heat transfer coefficient depends on the temperature difference between the solid and the environment as follows:

$$h_r = \varepsilon \sigma (\Theta + \Theta_0)(\Theta^2 + \Theta_0^2) \quad (4.11)$$

where σ is the Stefan-Boltzmann constant and ε is the emissivity of the material. Only the radiation to the ambient is modelled. The inner radiation in the machines is assumed to be negligible.

4.1.4 Thermal Network

When the thermal resistance of every part of the machine is defined. The resistances can be coupled together to form a complicated thermal network. Using circuit theory, a nodal analysis can be performed. A conductance matrix is created with the ambient temperature as the reference node. The temperature distribution can be found using the following equation

$$\Theta = \mathbf{K}_{node}^{-1} \mathbf{P}_{loss} + \Theta_0 \quad (4.12)$$

where Θ is a vector containing the temperatures at every node, \mathbf{P}_{loss} is a vector containing the power input at every node and Θ_0 is the environment temperature. The nodal conductance matrix \mathbf{K}_{node} is found as follows

$$\mathbf{K}_{node} = \begin{bmatrix} \sum_{i=1}^n \frac{1}{R_{1,i}} & -\frac{1}{R_{1,2}} & \cdots & -\frac{1}{R_{1,n}} \\ -\frac{1}{R_{2,1}} & \sum_{i=1}^n \frac{1}{R_{2,i}} & \cdots & -\frac{1}{R_{2,n}} \\ \vdots & \vdots & \ddots & \vdots \\ -\frac{1}{R_{n,1}} & -\frac{1}{R_{n,2}} & \cdots & \sum_{i=1}^n \frac{1}{R_{n,i}} \end{bmatrix} \quad (4.13)$$

where n is the number of nodes, the diagonal elements are the sum of the thermal conductances connected to the n^{th} node and $R_{i,j}$ is the thermal resistance between node i and j .

4.1.5 Assumptions

- There is no internal radiation from the stator to the rotor and vice versa.
- The thermal time-constant of the machines is assumed to be much higher than the period time of the ocean waves. With this assumption the heat capacities of the machines can be neglected.
- There is an independent radial and axial heat flow.
- There is no circumferential heat flow.

4.2 Iron-cored Generator

The iron cored machine is modelled using cylindrical components as described in section 4.1.1. The model for the iron cored machine is based on the lumped parameter model found in [33], but some changes were made since the model in [33] is of an induction machine.

4.2.1 Node Placement

When constructing a thermal model of an electrical machine, first the nodes have to be defined. Figure 4.3 shows the simplified thermal model of the IC-RF-PMSG, with all the nodes in place.

- | | | |
|-----------------|----------------------|-----------------|
| 1. stator yoke | 4. air gap | 7. rotor yoke |
| 2. stator teeth | 5. permanent magnets | 8. end windings |
| 3. windings | 6. rotor slots | |

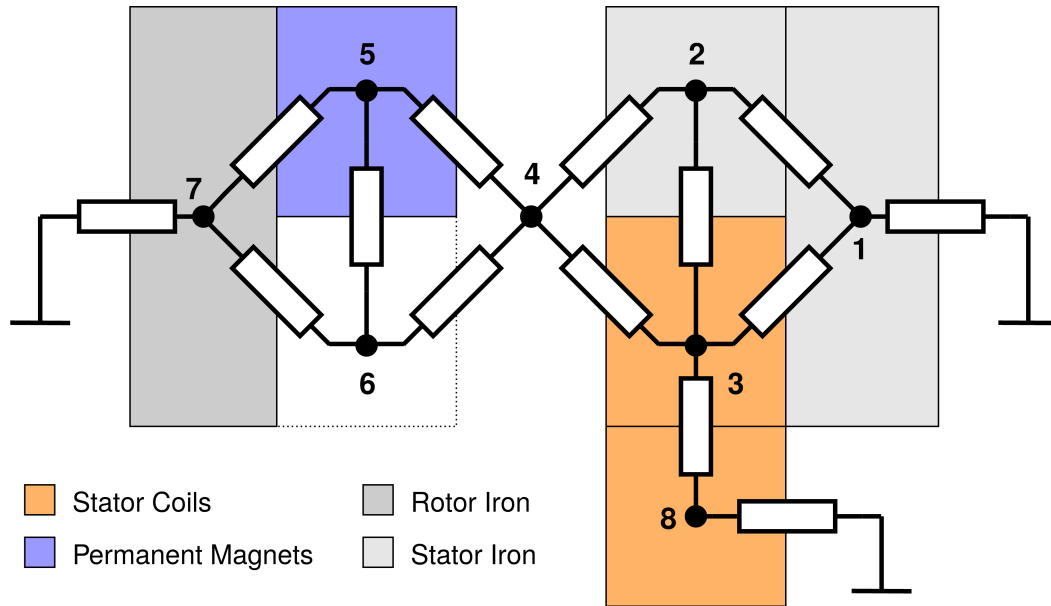


FIGURE 4.3: Node placement in the IC-RF-PMSG

The derivation of the thermal resistances and the detailed schematic of the thermal model is found in appendix C.1.

4.2.2 Stator

The stator consists of a stator yoke, stator teeth and the windings. Because of the iron laminations, the stator yoke and stator teeth have different thermal conductivities for the radial and axial direction. The amount of heat produced in the stator teeth and yoke are a consequence of the iron losses found with equations 3.22 and 3.23.

$$P_{node1} = \frac{P_{hy(sy)}}{2} + \frac{P_{ed(sy)}}{2} \quad P_{node2} = \frac{P_{hy(st)}}{2} + \frac{P_{ed(st)}}{2} \quad (4.14)$$

The stator windings are modelled as cylindrical rods lying in the slots. The windings are assumed to only conduct heat in the axial direction with thermal conductivity k_{cu} . The thermal conductivity in the radial direction is about 2.5 times the conductivity of the winding insulation k_v . This is empirically tested according to [33]. The slot liner is taken into account as well with thermal conductivity k_l . The amount of heat produced in the stator windings depends on the size of the stator winding with respect to the end windings. The rest of the copper losses are dissipated in the end windings.

$$P_{node3} = \frac{V_{coil}}{V_{cu}} \frac{P_{cu}}{2} \quad (4.15)$$

4.2.3 Air Gap

Since the rotor is moving relative to the stator, the air in the air gap is in motion. This affects the convection capabilities of the air gap. The air gap heat transfer coefficient can be expressed in terms of the Nusselt number Nu the conductivity of air k_{air} and the length of the air gap g .

$$h_g = \frac{k_{air}Nu}{g} \quad (4.16)$$

The Nusselt number for convection between two cylinders depends on the type of air flow in the air gap. The following derivation of the Nusselt number for different types of air flows is based on the method found in [34].

$$\begin{aligned} Nu &= 2 & Ta_m < 1700 & \text{ laminar flow} \\ Nu &= 0.128Ta_m^{0.367} & 1700 < Ta_m < 10^4 & \text{ transitional flow} \\ Nu &= 0.409Ta_m^{0.241} & 10^4 < Ta_m < 10^7 & \text{ turbulent flow} \end{aligned} \quad (4.17)$$

Here Ta_m is the modified Taylor number, which is found by dividing the Taylor number, Ta , by the geometrical factor F_g .

$$Ta_m = \frac{Ta}{F_g} \quad (4.18)$$

Ta and F_g are found as follows

$$Ta = \frac{\omega^2 g^3 D}{2v_{air}^2} \quad F_g = \frac{\pi^4 \frac{D-2.304g}{D-g}}{1697 \left(0.0056 + 0.0571 \left(\frac{D-2.304g}{D-g} \right)^2 \right) \left(1 - \frac{g}{D} \right)} \quad (4.19)$$

where ω is the angular velocity of the rotor, D is the air gap diameter and v_{air} is the kinematic viscosity of air.

4.2.4 Rotor

The heat from the air gap is transferred to the magnets proportional to the surface area of the magnets. The rest of the heat is transferred to the air in between the magnets which are modelled in a similar way as the magnets. The rotor yoke is modelled in the same way as the stator yoke. The only difference is that there are no laminations in the rotor iron, so thermal conductivity for the radial and axial direction are the same.

4.2.5 End Windings

The end windings are cooled by a fan connected to the rotor with an assumed efficiency of $\eta = 0.5$. The heat transfer coefficient of the end windings to the ambient air is calculated as follows.

$$h_{end} = 15.5 \left(1 + 0.29\eta\omega \frac{D}{2} \right) \quad (4.20)$$

where D is the air gap diameter and ω is the angular velocity of the rotor.

4.3 Air-cored Generator

In [36], a thermal model of an air-cored axial flux generator is shown. This model does not take the epoxy in the windings into account. In this section, the model from [36] is used as a basis with the addition of epoxy in the stator. Since the axial flux machine is symmetrical around the stator, only half of the machine needs to be modelled.

4.3.1 Node Placement

Figure 4.4 shows the placement of the nodes in the thermal model of the axial flux air cored machine.

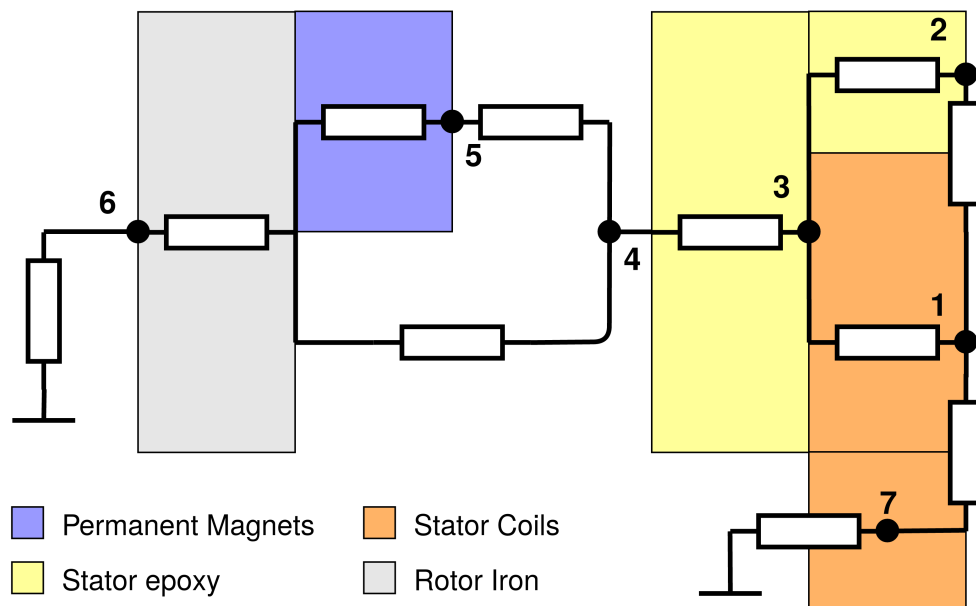


FIGURE 4.4: Node placement in the AC-AF-PMSG

- | | | |
|----------------|----------------------|-----------------|
| 1. windings | 4. air gap | 7. end windings |
| 2. epoxy teeth | 5. permanent magnets | |
| 3. epoxy layer | 6. rotor yoke | |

The derivation of the thermal resistances and the schematic of the thermal model is found in appendix C.2.

4.3.2 Stator

The stator of the air-cored machine is modelled as windings with epoxy teeth in between. On top of the stator is an epoxy layer which is in contact with the air gap.

The stator windings are modelled as rectangular cuboids. The windings have same thermal conduction properties as the windings of the iron-cored machine described in section 4.2.2. The amount of heat dissipated in the stator windings is the sum of the copper losses in the windings P_{cu} and the total amount of winding eddy currents P_{ed} . There are no eddy currents induced in the end windings since the end windings are not exposed to a changing magnetic field.

$$P = \frac{V_{coil}}{V_{cu}} \frac{P_{cu}}{2} + \frac{P_{ed}}{2} \quad (4.21)$$

4.3.3 Air gap

The air flow between two rotating disks is modelled differently than between two rotating cylinders. For a disk type machine, like the axial flux air-cored PMSG, the heat transfer coefficient can be calculated as follows

$$h_g = \frac{Nu k_{air}}{R_o} \quad (4.22)$$

where R_o is the outer diameter of the machine. The Nusselt number Nu is found using the Reynolds number. This method is based on the method found in [37]

$$Nu = 0.35 Re^{0.5} \quad (4.23)$$

The Reynolds number can be found as follows

$$Re = \frac{\omega R_o^2}{v_{air}} \quad (4.24)$$

4.3.4 Rotor

The rotor is modelled as a disk on which the permanent magnets are mounted. Both the rotor disk as the permanent magnets are modelled according to a one-dimensional model, where a single thermal resistance represents the conduction from the magnets to the rotor.

The convection from the rotor to the open air is divided into two parts, one from the rotor disks back and one at the rotor peripheral. The heat transfer coefficient at the back of the rotor disk can be found using the formula developed for a free rotating disk

$$h_{rb} = \frac{Nu_{rb}k_{air}}{R_o} \quad (4.25)$$

where R_o is the outer radius of the disk and, when there is a combination of laminar and turbulent air flow, the Nusselt number Nu_{rb} can be found using the following equation.

$$Nu_{rb} = 0.015Re^{\frac{4}{5}} - 100 \left(\frac{r_s}{R_o} \right)^2 \quad (4.26)$$

where the Reynolds number Re can be found using equation 4.24. r_c is the radius where the transition between the two air types of air flows occurs.

$$r_c = \sqrt{\frac{2.5 \times 10^5 v_a}{\omega}} \quad (4.27)$$

At the rotor peripheral, the heat transfer coefficient is found using the formula for a rotating cylinder in air

$$h_{rp} = \frac{Nu_{rp}k_{air}}{D_o} \quad Nu_{rp} = 0.013Re^{\frac{2}{3}} - Pr^{\frac{1}{3}} \quad (4.28)$$

Again, the Reynolds number Re is found using equation 4.24. Pr is the Prandtl number, which is about 0.7 for air.

4.3.5 End Windings

The end windings in the air-cored generator are also cooled by a fan. The heat transfer coefficient is calculated using equation 4.20.

Chapter 5

Optimization

With the models for both generators in place, the generators can be compared to each other. For a good comparison, the generators should have an optimal design for which they are as efficient and cheap as possible. The following chapter describes the optimization process.

5.1 Optimization Variables and Constraints

The design variables defined in section 3.1 and presented in table 5.1 are used as the optimization variables. By varying the values of these variables within a certain range, the optimal design can be found.

TABLE 5.1: Optimization variables

Iron-cored	Symbol	Air-cored	Symbol
magnet width to pole pitch ratio	α	inner to outer diameter	λ
machine length	l_s	magnet width to pole pitch ratio	α
air gap diameter	D	outer diameter	D_o
slot height	h_s	slot height	h_s
number of poles	p	number of poles	p
magnet height	h_m	magnet height	h_m
stator yoke height	h_{sy}		
tooth width to slot width ratio	β		

To ensure the optimized generators meet the specifications, the following non-linear constraints are defined:

$$\begin{aligned}
T_{max} &> T_{spec} \\
\Theta_{cu} &< \Theta_{cu,max} \\
\hat{B}_s &< \hat{B}_{g1} - B_{min} \\
\Theta_{pm} &< \Theta_{pm,max}
\end{aligned} \tag{5.1}$$

These constraints imply that the design is only accepted when the maximum torque the machine is able to produce, T_{max} , is higher than the rated torque T_{spec} . The winding temperature Θ_{cu} should not exceed the rated maximum temperature Θ_{max} . In order to prevent demagnetization of the magnets, the field produced by the stator current, \hat{B}_s , should not cause the field in the magnets to be lower than the minimum value before demagnetization B_{min} . Also, the temperature in the magnets should not be higher than the maximum temperature before demagnetization $\Theta_{pm,max}$.

5.2 Optimization Objective

The generators are tested on both efficiency and costs. To compare efficiency with costs, the efficiency is expressed in costs as well. The losses can be seen as kilowatt hours which could have been sold. The following expression brings the two criteria together.

$$C = C_{gen} + P \times E_{dis} \times C_{kWh} \tag{5.2}$$

C_{gen} represents the cost of the generators active material, P a period of time in which an additional investment in the generator should be earned back, E_{dis} the annually dissipated energy and C_{kWh} the price of one kilowatt hour.

The aim for the optimization function is to keep the optimization objective C as low as possible. The generator with the lowest overall costs will be the best choice for the Symphony.

The price at which one kilowatt hour can be sold lies higher for subsidized energy sources than for conventional energy sources. In order to boost new renewable energy sources, a feed-in tariff is used. This system allows independent electricity producers to feed renewable energy into the grid at a fixed tariff for a determined period of time. In Portugal, the feed-in tariff is at 0.26 €/kWh for a period of 15 years [38].

In this optimization procedure, the geometry of the Symphony is assumed to be fixed. When the generator is implemented in the system, the material costs of the rest of the system should be taken into account in the optimization procedure as well. An

additional investment in generator materials might make the generator more efficient, but the same investment could make the whole system even more efficient when placed in one of the other mechanical parts.

5.3 Wave Spectrum Implementation

Appendix A shows the scatter diagram of Leixous in Portugal. On the horizontal axis the wave period time T_e is found, on the vertical axis the specific wave height H_s . For every combination of H_s and T_e , the probability of occurrence can be found. In order to find the annually dissipated energy E_{dis} , the dissipated power per sea state is multiplied by the rate of occurrence per sea state. A time domain model is present which gives the output power of the turbine of the Symphony at every given combination of significant wave height and wave period time. With this parameter as an input to the generator, the analytical models can calculate the losses for every sea state. Figure 5.1 shows the optimization process in a flowchart.

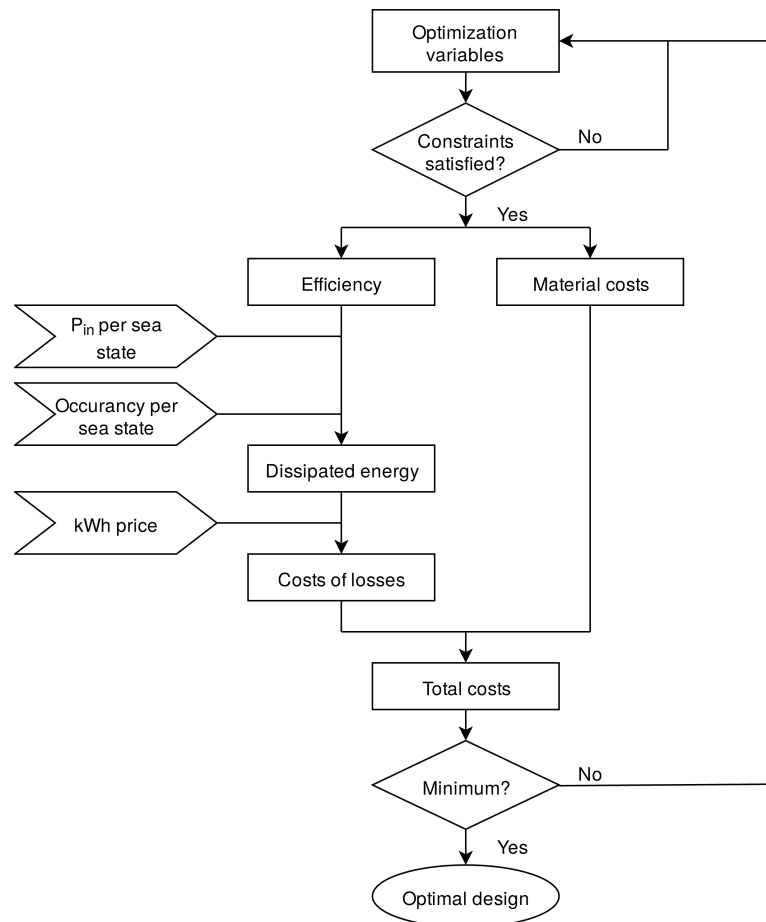


FIGURE 5.1: Optimization process flow

Chapter 6

Results

In this chapter, the results of the optimization procedure are presented and discussed. First the geometries of the optimized generators are shown. Then the optimized generators are tested on efficiency, material costs and thermal capabilities.

6.1 Optimized Design

Table 6.1 shows optimized design variables for both the radial flux iron-cored and the axial flux air-cored machine.

TABLE 6.1: Optimized variables

Iron-cored	Value	Unit	Air-cored	Value	Unit
D	800	mm	D_o	800	mm
l_s	61.1	mm	l_s	126.1	mm
			λ	0.67	
p	16		p	8	
h_m	3.7	mm	h_m	4.4	mm
τ_p	83.8	mm	τ_{pi}	107.6	mm
b_m	34.5	mm	b_m	106.4	mm
α	0.44		α	0.99	
h_s	26.6	mm	h_s	4.3	mm
b_s	15.9	mm	b_s	35.9	mm
b_t	12.0	mm			
β	0.43				
h_{sy}	126	mm			

Both the optimization for the iron-cored and the air-cored generator tends to maximize the diameter of the machines to the upper bound of 0.8 m. The magnet thickness is restricted by the demagnetization constraint. The rest of the variables are all within their restrictions.

6.2 Results of the Analytical Model

Table 6.2 shows some of the generators parameters for an input power of $P_{in} = 2.5$ kW.

TABLE 6.2: Generator dimensions

Symbol	IC	AC	Unit	Symbol	IC	AC	Unit
E	195	236	V	I_s	4.16	3.50	A
T	67	67	Nm	n	350	350	rpm
R_s	0.43	0.35	Ω	N_s	40	18	
\hat{B}_{g1}	0.28	0.71	T	k_l	0.97	0.97	
m_{pm}	1.9	14.7	kg	m_{cu}	30.0	8.0	kg
m_{fe}	212	114	kg	m_{tot}	243	136	kg

As expected, the air-cored generator needs more permanent magnetic material than the iron-cored generator. The air-cored generator uses almost 8 times more permanent magnetic material than the iron-cored generator.

There is a notable difference in air gap flux density, \hat{B}_{g1} , between both machines. While the optimization for the air-cored machine tries to keep the air gap flux density at a high level, the optimization for the iron-cored machine seems to suppress the air gap flux density. A possible explanation for this phenomenon could be that the optimization is trying to reduce iron losses, since $P_{hy} \propto \hat{B}^{1.6}$ and $P_{ed} \propto \hat{B}^2$. Apparently, it is cheaper to reduce the air gap flux density and compensate for this with more windings per slot, N_s , and copper, m_{cu} .

The iron-cored generator is almost twice as heavy as the air-cored generator. Only the weights of the active materials are taken into account though, there might also be a difference in structural weights.

6.3 Results of the Thermal Model

Table 6.3 shows the temperature distributions of the optimized air-cored and iron-cored generator at the maximum average input power of $P_{in} = 11$ kW.

TABLE 6.3: Temperature distribution

Symbol	IC	AC	Unit	Symbol	IC	AC	Unit
Θ_{sy}	39.9		$^{\circ}\text{C}$	Θ_{st}	44.9		$^{\circ}\text{C}$
Θ_{cu}	51.0	36.2	$^{\circ}\text{C}$	Θ_{ep}		35.9	$^{\circ}\text{C}$
Θ_g	40.3	28.7	$^{\circ}\text{C}$	Θ_{pm}	23.8	21.7	$^{\circ}\text{C}$
Θ_{ry}	23.0		$^{\circ}\text{C}$				

Both the iron-cored and the air-cored winding and magnet temperature do not exceed the limits at the maximum power.

Figure 6.1 shows the winding temperature of both machines for a range of input powers.

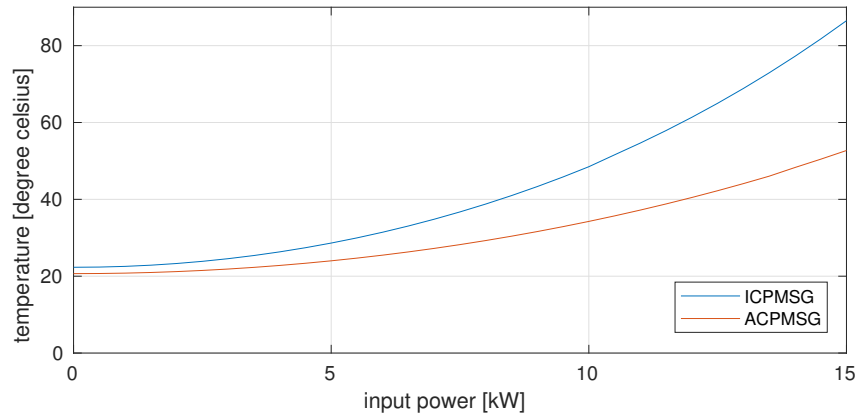


FIGURE 6.1: Winding temperature

The air-cored generator shows better cooling properties than the iron-cored generator.

6.4 Losses and Costs

Figure 6.2 shows the efficiencies of both generators for different input powers at $n = 350$ rpm.

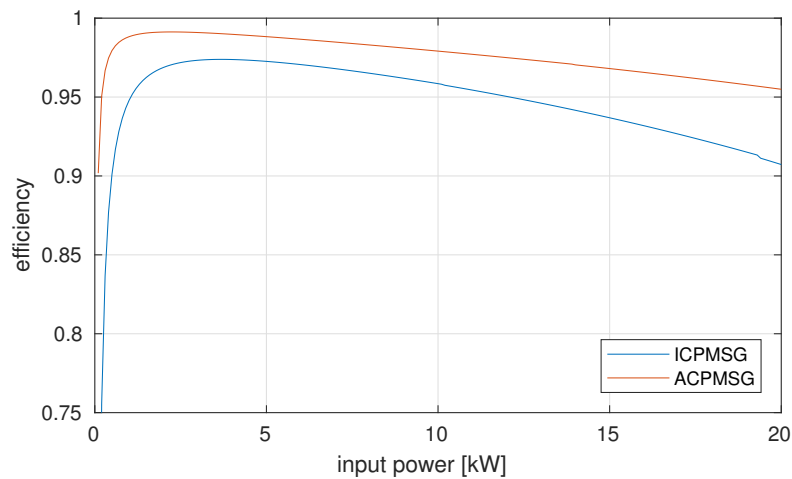


FIGURE 6.2: Efficiency over a power range

This graph clearly shows the air-cored generator is more efficient than the iron-cored generator, especially for the lower powers. The iron losses are relatively high in this area, so the iron-cored generator loses efficiency. In the higher power range, both generators efficiencies drop. This is due to the heating of the windings, which increases the windings resistance.

Table 6.4 shows the individual losses of both generators for an input power of $P_{in} = 2.5$ kW. The table also shows the costs of the different materials used in the generators.

TABLE 6.4: Losses and costs

Symbol	IC	AC	Unit	Symbol	IC	AC	Unit
P_{cu}	21.3	12.1	W	C_{pm}	138	610	€
$P_{fe(ed)}$	18.0		W	C_{cu}	404	127	€
$P_{fe(hy)}$	30.7		W	C_{fe}	620	335	€
$P_{cu(ed)}$		9.8	W	C_{tot}	1164	1072	€

The amount of iron losses in the iron-cored generator are relatively high with respect to the copper losses. This is because the input power of 2.5 kW is under normal operating conditions. The generator is rated at 11 kW, however.

As expected, the air-cored generator needs more permanent magnetic material than the iron-cored generator. This is a significant part of the total costs of the generator. The iron-cored generator, on the other hand, needs more copper and iron. Though it was expected that the materials of the air-cored generator would be more expensive, the materials costs of the iron-cored and air-cored generator are roughly the same.

Figure 6.3 shows the efficiencies of both generators for a half wave cycle of the Symphony.

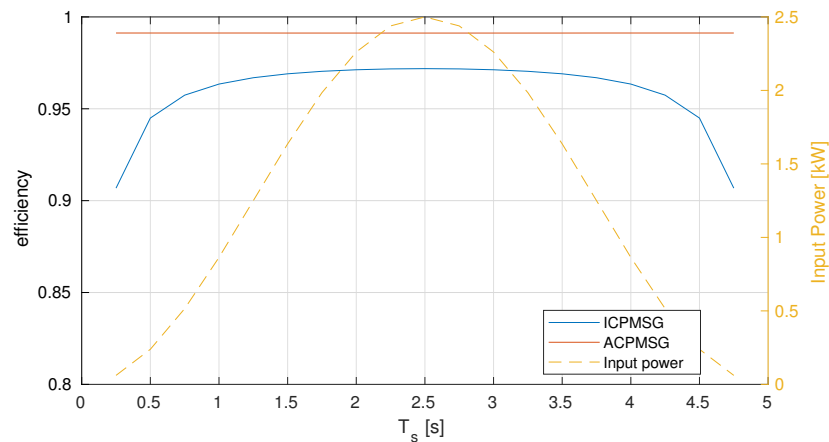


FIGURE 6.3: Efficiency per wave cycle

The air-cored generator has the same efficiency over the whole wave cycle. The iron-cored generator decreases in efficiency at lower input powers. This is because the hysteresis losses in the iron are proportional to the electric frequency. This effect is not really significant though since most of the power is concentrated in the range where the iron-cored machine is most efficient.

Finally, in order to determine the best generator for the Symphony, the optimization criteria have to be compared. Table 6.5 shows the optimization criterion for both generators.

TABLE 6.5: Optimization criterion

Description	Symbol	IC	AC	Unit
Material costs	C_{mat}	1164	1072	€
Cost of losses	C_{loss}	4482	2141	€
Optimization criterion	C	5646	3213	€

From these results, it is clear that the axial flux air-cored generator is a cheaper solution than the radial flux iron-cored generator. Not only are the material costs of the air-cored generator slightly less, it also dissipates almost half of the power the iron-cored generator does under the same conditions.

The results were generated with the assumption that the feed-in tariff, described in section 5.2, is 0.26 €/kWh. In order to analyze the sensitivity of the criterion, a few optimizations were done for different feed in tariffs. The results are shown in figure 6.4.

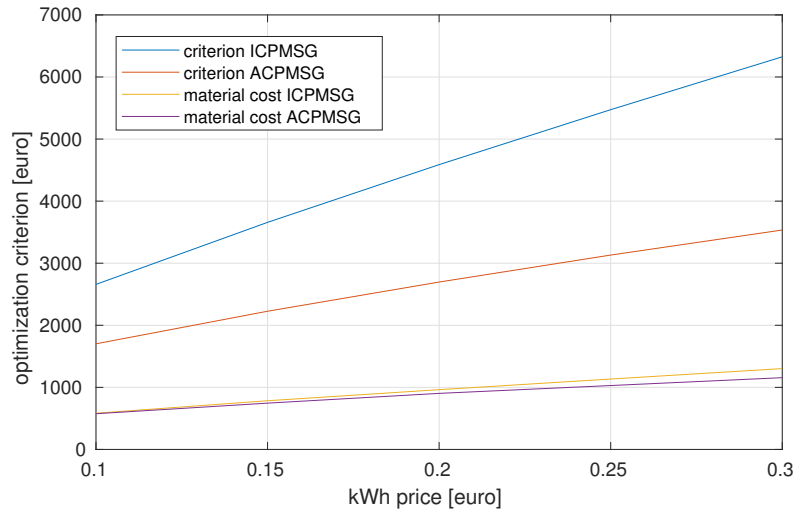


FIGURE 6.4: Optimization for different kWh prices

Even if the feed-in tariff would be higher or lower, the axial flux air-cored still is the best option for the Symphony Wave Power device.

Chapter 7

Conclusions and Recommendations

The following chapter concludes this thesis. Recommendations and further research are discussed as well.

7.1 Conclusions

The aim of this research is to find the best generator design for the Symphony wave energy converter. The generator should be efficient, cheap, and reliable. There is some research available on generator designs for wave energy converters (WEC). Depending on the WEC, different generator types, for example synchronous or induction generators are chosen. Like many WEC's, the Symphony is a unique case so a separate research was needed here as well.

Several generator types are suitable for the Symphony. Compared to induction and switched reluctance generators, a radial flux iron-cored permanent magnet synchronous generator (PMSG) seems a good choice because it is efficient and reliable. A disadvantage of the iron-cored PMSG, though, is that, in the case of the Symphony, the iron losses are relatively high at partial loads. An axial flux air-cored PMSG does not have this problem since there are no iron losses at all. A drawback of the axial flux air-cored PMSG, however, is that it needs more permanent magnetic material than an iron-cored generator which increases costs. It was decided to test the iron-cored radial flux PMSG and the air-cored axial flux PMSG on both efficiency and material costs.

In order to compare the axial flux air-cored PMSG to the radial flux iron-cored PMSG, an analytical model was built which puts out efficiency and material cost and temperatures

of both an air-cored and an iron-cored PMSG. To find the best generator geometries for the case of the Symphony, an optimization procedure was created which minimizes both material costs and losses.

It was found that an axial flux air-cored PMSG is more efficient than a radial flux iron-cored PMSG. The iron losses of an iron-cored generator are relatively high at partial loads while the Symphony operates at partial loads most of the time. Moreover, the active materials for an air-cored PMSG are also cheaper than for an iron-cored PMSG. In conclusion: the best generator design for the Symphony Wave Power device is an axial flux air-cored permanent magnet synchronous generator.

7.2 Recommendations and Further Research

In this thesis, only the material cost of the generators are taken into account. For a better comparison, the costs of the construction materials and the production of the generators should be taken into account as well. There are some geometrical differences between the air-cored and iron-cored generator, so there will be a difference in costs as well. As stated in section 5.2, the optimization procedure can be improved by taking the total costs of the Symphony into account.

The assumptions that were made for the analytical models simplify the models but reduce the accuracy. While it is assumed that the models are accurate enough, the models could be improved by including higher harmonics, magnet and rotor iron losses, mechanical losses, etc. This will increase the computing time of the optimization procedure. The choices that have to be made in modelling a generator, will mostly be a compromise between accuracy and computing time or complexity.

In section 2.3.3 it was found that the switched reluctance generator could also be an attractive solution as a generator for the Symphony. A model of the SRG can be build to compare this topology to the iron-cored and air-cored generator.

The Symphony has a high peak-to-average power ratio and the requirement to act as a braking device during extreme weather conditions. This causes the Symphony to need an overrated generator during normal operation. An investigation in the overloading of generators could give an extra perspective on how large the generator eventually has to be. Saturation of iron, thermal properties and demagnetization play an important role here.

The main purpose of the Symphony is to make the production of electrical energy more sustainable. The mining of permanent magnets is controversial however [39]. The air-cored generator uses more permanent magnet material than its iron cored counter part, so it would be wise to do a research on the origin of permanent magnet material and the impact on the environment.

The air-cored generator can also be used as a linear generator, which could be placed in a direct drive wave energy converter. This could improve the overall efficiency of the WEC in the same way as for the Symphony since there are no iron losses. One of the problems with the design of a linear generator based WEC are the mechanical forces between the stator and translator. An air-cored generator does not have any magnetic material in the stator. This will decrease the force between the rotor and translator.

Bibliography

- [1] Falnes J. *A review of wave-energy extraction*, Marine Structures 20, 2007, 185-201.
- [2] Clément A, McCullen P, Falção A, Fiorentino A, Gardner F, Hammarlund K, Lemois G, Lewis T, Nielsen K, Petroncini S, Pontes M, Schild B, Jöström P, Sørensen H and Thorpe, T. *Wave energy in Europe: current status and perspectives*, Renew. Sust. Energy Rev., 2002, 6(5), 405-431.
- [3] Falção A. *Wave energy utilization: A review of the technologies* Renew. Sust. Energy Rev., 2010, 14(3), 899-918.
- [4] Drew B, Plummer AR, Sahinkaya MN. *A review of wave energy converter technology*, Proc Inst Mech Eng Part A-J Power Energy 2010, 223:887-902.
- [5] Polinder H, Mecrow B, Dickinson P, Mueller M *Linear generators for direct-drive wave energy conversion* Proc. IEEE Int. Electric Machines Drives Conf. vol. 2, 2003, 798804.
- [6] Datta R, Ranganathan V *Variable-speed wind power generation using a double fed wound rotor induction machine: a comparison with alternative schemes* IEEE Power Engineering Review, vol. 22, no. 7, pp. 52-52, 2002
- [7] Beainy A, Maatouk C, Moubayed N, Kaddah F *Comparison of different types of generator for wind energy conversion system topologies* 3rd Int. Conf. on Renew. Energ. for Developing Countries, 2016
- [8] Muller N, Kouro S, Glaria J, Malinowski M *Medium-voltage power converter interface for Wave Dragon wave energy conversion system* Proceedings of the IEEE ECCE, Denver (USA), pp. 352-358, 2013
- [9] Henderson R *Design, simulation, and testing of a novel hydraulic power take-off system for the Pelamis wave energy converter* Renewable Energy, vol. 31, no. 2, pp. 271-283, 2006

-
- [10] O’Sullivan D, Lewis A *Generator selection and comparative performance in offshore oscillating water column ocean wave energy converters* IEEE Transactions on Energy Conversion, vol. 26, no. 2, pp. 603-614, 2011
- [11] Henriques J, Gato L, Lemos J, Gomes R, Falcao A *Peak-power control of a grid-integrated oscillating water column wave energy converter* Energy, vol. 109, pp. 378-390, 2016
- [12] Jayashankar V, Udayakumar K, Karthikeyan B, Manivannan K, Venkatraman N, Rangaprasad S *Maximizing power output from a wave energy plant* Power Engineering Society Winter Meeting, vol. 3, pp. 1796-1801, 2000
- [13] Kiran D, Palani A, Muthukumar S, Jayashankar V *Steady grid power from wave energy* IEEE Transactions on Energy Conversion, vol. 22, no. 2, pp. 539-540, 2007
- [14] Marques G *Stability study of the slip power recovery generator applied to the sea wave energy extraction* IEEE Power Electronics Specialists Conference, vol. 1, pp. 732-738, 1992
- [15] Polinder H, Damen M, Gardner F *Linear PM generator system for wave energy conversion in the AWS* IEEE transactions on energy conversion, VOL. 19, NO. 3, 2004, 583-589
- [16] Mueller M *Electrical generators for direct drive wave energy converters* IEE Proc.-Gener. Transm. Distrib., Vol. 149, No. 4, 2002, 446-456
- [17] Al-Saffar M, Nho E, Lipo A *Controlled shunt capacitor self-excited induction generator* Conf. Rec. IEEE Industry Applications Conf. vol 2, pp. 1486-1490, 1998
- [18] Estanislao E, Ozan K, Mueller M *Rotor loss prediction in air-cored permanent magnet machines* Conference paper, 2013, DOI:10.1109/IEMDC.2013.6556268
- [19] Parviainen A *Design of axial-flux permanent-magnet low-speed machines and performance comparison between radial-flux and axial-flux machines* ISSN 1456-4491, 2005
- [20] Saho N, Xu X, Panda S *Low torque ripple control of using iterative learning* IEEE Transactions on Energy Conversion, vol. 16, no. 4, pp. 318-326, 2001.
- [21] Ramakrishnan K, Curti M, Zarko D, Mastinu G, Paulides J, Lomonova E *Comparative analysis of various methods for modelling surface permanent magnet machines*
- [22] Polinder H, Slootweg J, Hoeijmakers M, Compter J *Modeling of a linear PM machine including magnetic saturation and end effects: maximum force-to-current ratio* IEEE transactions on industry applications, vol. 39, no. 6, pp. 1681-1688, 2003

- [23] Pyrhonen J, Jokinen T, Hrabovcov V *Design of rotating electrical machines* Chippingham, Great Britain, Wiley, 2008
- [24] Hanselman D *Magnetic Modelling in Brushless Permanent Magnet Motor Design* 2nd ed. Cranston: Writers Collective, 2003, ch. 2
- [25] Grauers A *Design of Direct-driven Permanent-magnet Generators for Wind Turbines* ISSN 0346-718X, 1996
- [26] Xuan H, Lahaye D, Polinder H, Ferreira J *Influence of Stator Slotting on the Performance of Permanent-Magnet Machines with Concentrated Windings* ISSN 1389-6520, 2012
- [27] Qu R, Lipo T *Analysis and Modeling of Air-Gap and Zigzag Leakage Fluxes in a Surface-Mounted Permanent-Magnet Machine* IEEE Transactions on Industry Applications, VOL. 40, 2004, 121-127
- [28] Daghigh A, Javadi H, Torkaman H *Optimal Design of Coreless Axial Flux Permanent Magnet Synchronous Generator with Reduced Cost Considering Improved PM Leakage Flux Model* Electric Power Components and Systems, 45:3, 264-278
- [29] Kamper M, Wang R, Rossouw F *Analysis and performance of axial flux permanent-magnet machine with air-cored nonoverlapping concentrated stator windings* IEEE transactions on industry applications, vol. 44, no. 5, 2008
- [30] Wang R, Kamper M *Calculation of Eddy Current Loss in Axial Field Permanent-Magnet Machine With Coreless Stator* IEEE Transactions on Energy Conversion, VOL. 19, NO. 3, 2004, 532-538
- [31] Zhang, Z *Ironless permanent magnet generators for direct-driven offshore wind turbines* ISSN 1503-8181, 2015
- [32] Wang R *Design aspects and optimisation of an axial field permanent magnet machine with an ironless stator* Ph.D. dissertation, Dept. Elect. Eng., Univ. Stellenbosch, Matieland, South Africa, 2003.
- [33] Mellor P, Roberts D, Turner D *Lumped parameter thermal model for electrical machines of TEFC design* IEE Proceedings-B, Vol. 138, NO. 5, 1991
- [34] Nerg J, Rilla M, Pyrhönen H *Thermal analysis of radial-flux electrical machines with a high power density* IEEE Transactions on industrial electronics, VOL. 55, NO. 10, 2008, 3543-3554
- [35] Rostami N, Feyzi M, Pyrhönen J, Parviainen A, Niemelä *Lumped-parameter thermal model for axial flux permanent magnet machines* IEEE transactions on magnetics, vol. 49, no. 3, pp. 1178-1184, 2013

-
- [36] Gieras J, Wang R, Kamper M *Cooling and heat transfer in Axial flux permanent magnet brushless machines* Dordrecht, The Netherlands: Kluwer, 2004, ch. 8, pp. 249-279.
- [37] Howey D, Childs P, Holmes A *Air-gap convection in rotating electrical machines* IEEE Transactions on industrial electronics, VOL. 59, NO. 3, 2012, 1367-1375
- [38] Rousseau N *Ocean Energy: a european perspective* [Online]. Available: http://www.wavec.org/content/files/eu-oea_1108_WAVEC_workshop.pdf
- [39] Kaiman J *Rare earth mining in China: the bleak social and environmental costs* [Online]. Available: <https://www.theguardian.com/sustainable-business/rare-earth-mining-china-social-environmental-costs>

Appendix A

Wheater Conditions Leixous

P[Hs vs Te] (%)	=< 0.5m	0.5-1m	1-1.5m	1.5-2m	2-2.5m	2.5-3m	3-3.5m	3.5-4m	4-4.5m	4.5-5m	5-6m	6-7m	7-8m	8-9m	9-10m	10-12m	P[Te]
=< 4 s																	0.0
4 - 5 s		0.07	0.03														0.1
5 - 6 s		2.41	4.53	1.73	0.23												8.9
6 - 7 s		2.21	10.14	7.04	2.57	0.59	0.03										22.6
7 - 8 s		0.33	5.8	7.22	3.77	2.01	0.99	0.18	0.01								20.3
8 - 9 s		0.01	2.03	5.39	4.28	2.82	1.74	1.05	0.53	0.11							18.0
9 - 10 s			0.38	2.29	3.78	2.52	1.77	1.43	0.83	0.6	0.36						14.0
10 - 11 s			0.05	0.34	1.77	1.88	1.35	1.12	0.75	0.7	0.83	0.17	0.03				9.0
11 - 12 s			0.01	0.12	0.41	0.71	0.52	0.7	0.51	0.55	0.61	0.34	0.07	0.01			4.6
12 - 13 s					0.05	0.13	0.23	0.16	0.22	0.29	0.33	0.18	0.13	0.05	0.03		1.8
13 - 14 s						0.01	0.05	0.06	0.08	0.1	0.07	0.06	0.05	0.09	0.05	0.01	0.6
14 - 15 s									0.01	0.01	0.03	0.05	0.02	0.03		0.01	0.2
15 - 16 s															0.01		0.0
16 - 17 s															0.01		0.0
17 - 18 s																	0.0
18 - 19 s																	0.0
19 - 20 s																	0.0
20 - 21 s																	0.0
21 - 22 s																	0.0
> 22 s																	0.0
P[Hs] (%)	0.0	5.0	23.0	24.1	16.9	10.7	6.7	4.7	2.9	2.4	2.2	0.8	0.3	0.2	0.1	0.0	100

FIGURE A.1: Scatter diagram

Appendix B

Used Numbers

General

Description	Symbol	Unit	Value
vacuum permeability	μ_0	Hm^{-1}	$4\pi \times 10^{-7}$
Stephan-Boltzmann constant	σ	Wm^{-2}K^4	5.67×10^{-8}
room temperature	Θ_0	K	293.15

Air

Description	Symbol	Unit	Value
density	ρ	kgm^{-3}	1.225
relative permeability	μ_r	-	1
kinematic viscosity	ν	m^2s^{-1}	1.51×10^{-5}
thermal conductivity	k	$\text{WK}^{-1}\text{m}^{-1}$	0.024
Prandtl number	Pr	-	0.7

Copper

Description	Symbol	Unit	Value
specific cost	c	€kg^{-1}	15
density	ρ	kgm^{-3}	8900
relative permeability	μ_r	-	1
resistivity	ρ	$\Omega \text{ m}$	1.68×10^{-8}
fill factor air-cored	k_f	-	0.45
fill factor iron-cored	k_f	-	0.585
temperature coefficient	α	-	0.004041
thermal conductivity	k	$\text{WK}^{-1}\text{m}^{-1}$	401
varnish conductivity	k_v	$\text{WK}^{-1}\text{m}^{-1}$	0.26
slot liner conductivity	k_i	$\text{WK}^{-1}\text{m}^{-1}$	

insulation thickness	d_i	mm	0.035
radial conductivity factor	F	-	2.5

Permanent magnets (Nd-Fe-B)

Description	Symbol	Unit	Value
specific cost	c	€	40
density	ρ	kgm ⁻³	7500
remenance flux density	B_r	T	1.15
relative permeability	μ_r	-	1.05
thermal conductivity	k	WK ⁻¹ m ⁻¹	8.95

Electrical steel

Description	Symbol	Unit	Value
specific cost	c	€kg ⁻¹	3
density	ρ	kgm ⁻³	7874
relative permeability	μ_r	-	∞
specific eddy current losses	$P_{0(ed)}$	Wkg ⁻¹	0.76
specific hysteresis losses	$P_{0(hy)}$	Wkg ⁻¹	2.04
loss factor eddy currents in teeth	$k_{st(ed)}$	-	2.5
loss factor eddy currents in yoke	$k_{sy(ed)}$	-	1.8
loss factor hysteresis in teeth	$k_{st(hy)}$	-	1.2
loss factor hysteresis in yoke	$k_{sy(hy)}$	-	2
axial thermal conductivity	k_a	WK ⁻¹ m ⁻¹	3.7
radial thermal conductivity	k_r	WK ⁻¹ m ⁻¹	38.7

Construction steel

Description	Symbol	Unit	Value
specific cost	c	€kg ⁻¹	3
thermal conductivity	k	WK ⁻¹ m ⁻¹	50
density	ρ	kgm ⁻³	7874
relative permeability	μ_r	-	∞

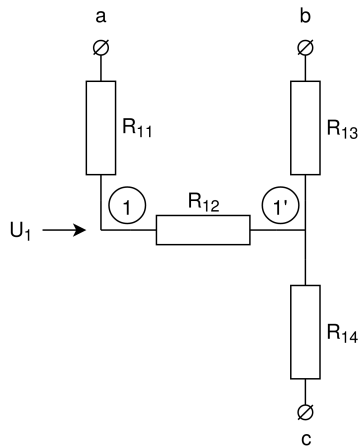
TABLE B.1: Your caption here

Appendix C

Thermal Models

C.1 Iron-Cored Generator

C.1.1 Stator Yoke



- a: to ambient in axial direction
- b: to ambient in radial direction
- c: to stator teeth and windings in axial direction

FIGURE C.1: Node 1: stator yoke

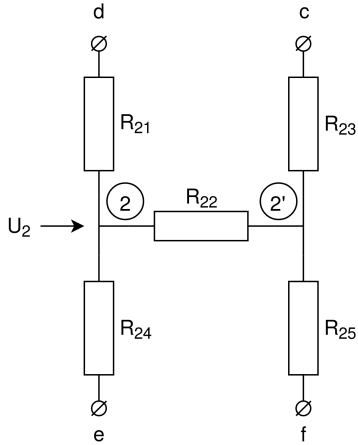
$$R_{11} = \frac{l_s}{6\pi k_{la}(r_o^2 - r_i^2)}$$

$$R_{12} = \frac{-1}{4\pi k_{lr} l_s (r_o^2 - r_i^2)} \left[r_o^2 + r_i^2 - \frac{4r_o^2 r_i^2 \ln\left(\frac{r_o}{r_i}\right)}{r_o^2 - r_i^2} \right]$$

$$R_{13} = \frac{1}{2\pi k_{lr} l_s} \left[1 - \frac{2r_i^2 \ln\left(\frac{r_o}{r_i}\right)}{r_o^2 - r_i^2} \right]$$

$$R_{14} = \frac{1}{2\pi k_{lr} l_s} \left[\frac{2r_o^2 \ln\left(\frac{r_o}{r_i}\right)}{r_o^2 - r_i^2} - 1 \right]$$

C.1.2 Stator Teeth



- d: to ambient in axial direction
- c: to stator yoke in radial direction
- e: to windings in axial direction
- f: to air gap in radial direction

FIGURE C.2: Node 2: stator teeth

$$R_{21} = \frac{\tau_s l_s}{b_t 6\pi k_{la} (r_o^2 - r_i^2)}$$

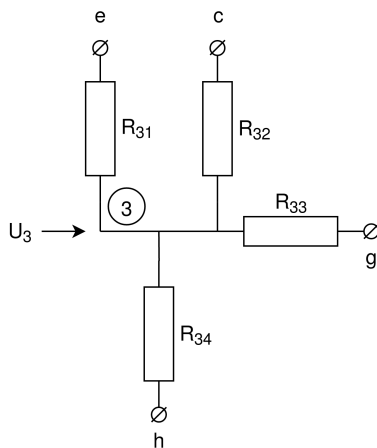
$$R_{22} = \frac{-\tau_s}{b_t 4\pi k_{lr} l_s (r_o^2 - r_i^2)} \left[r_o^2 + r_i^2 - \frac{4r_o^2 r_i^2 \ln\left(\frac{r_o}{r_i}\right)}{r_o^2 - r_i^2} \right]$$

$$R_{23} = \frac{\tau_s}{b_t 2\pi k_{lr} l_s} \left[1 - \frac{2r_i^2 \ln\left(\frac{r_o}{r_i}\right)}{r_o^2 - r_i^2} \right]$$

$$R_{24} = \frac{b_t \pi (r_o^2 - r_i^2)}{\tau_s k_{lr} l_s (r_o - r_i)^2 Q_s^2}$$

$$R_{25} = \frac{\tau_s}{b_t 2\pi k_{lr} l_s} \left[\frac{2r_o^2 \ln\left(\frac{r_o}{r_i}\right)}{r_o^2 - r_i^2} - 1 \right]$$

C.1.3 Stator Windings



- e: to stator teeth
- c: to stator yoke
- g: to endwindings
- h: to air gap

FIGURE C.3: Node 3: stator windings

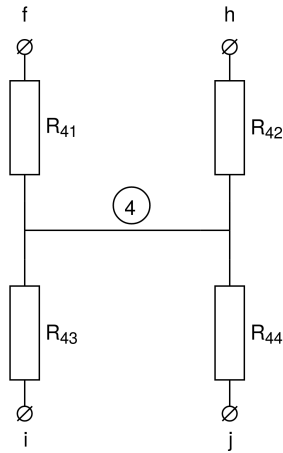
$$R_{31} = \frac{2d_i}{\pi k_i l_s r_{cu} Q_s} + \frac{1}{2\pi k_v l_s F Q_s}$$

$$R_{32} = \frac{4d_i}{\pi k_i l_s r_{cu} Q_s} + \frac{1}{\pi k_v l_s F Q_s}$$

$$R_{33} = \frac{l_s}{6k_{cu} A_{cu} Q_s}$$

$$R_{34} = \frac{1}{\pi k_v l_s F Q_s}$$

C.1.4 Air Gap



- f: to stator teeth
- h: to stator windings
- i: to permanent magnets
- j: to rotor slots

FIGURE C.4: Node 4: air gap

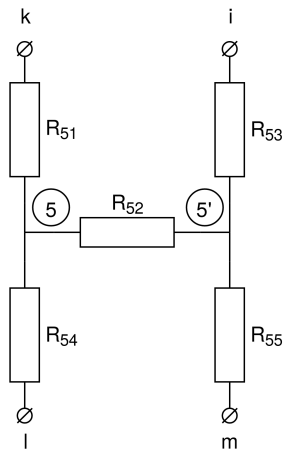
$$R_{41} = \frac{\tau_s}{b_t \pi r_o l_s h_g}$$

$$R_{42} = \frac{\tau_s}{b_s \pi r_o l_s h_g}$$

$$R_{43} = \frac{\tau_p}{b_m \pi r_o l_s h_g}$$

$$R_{44} = \frac{\tau_p}{b_{rs} \pi r_o l_s h_g}$$

C.1.5 Permanent Magnets



- k: to ambient
- i: to air gap
- l: to rotor slots
- m: to rotor yoke

FIGURE C.5: Node 5: permanent magnets

$$R_{51} = \frac{\tau_p l_s}{b_m 6\pi k_m (r_o^2 - r_i^2)}$$

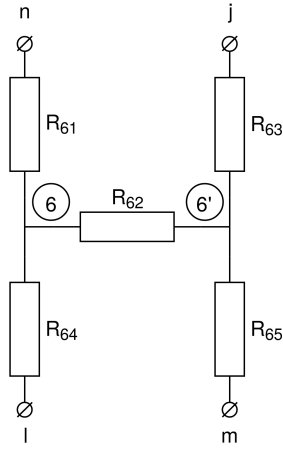
$$R_{52} = \frac{-\tau_p}{b_m 4\pi k_m l_s (r_o^2 - r_i^2)} \left[r_o^2 + r_i^2 - \frac{4r_o^2 r_i^2 \ln\left(\frac{r_o}{r_i}\right)}{r_o^2 - r_i^2} \right]$$

$$R_{53} = \frac{\tau_p}{b_m 2\pi k_m l_s} \left[1 - \frac{2r_i^2 \ln\left(\frac{r_o}{r_i}\right)}{r_o^2 - r_i^2} \right]$$

$$R_{54} = \frac{b_m \pi (r_o^2 - r_i^2)}{\tau_p k_m l_s (r_o - r_i)^2 Q_s^2}$$

$$R_{55} = \frac{\tau_p}{b_m 2\pi k_m l_s} \left[\frac{2r_o^2 \ln\left(\frac{r_o}{r_i}\right)}{r_o^2 - r_i^2} - 1 \right]$$

C.1.6 Rotor Slots



k: to ambient

i: to air gap

l: to permanent magnets

m: to rotor yoke

FIGURE C.6: Node 6: rotor slots

$$R_{61} = \frac{\tau_p l_s}{b_{rs} 6\pi k_a (r_o^2 - r_i^2)}$$

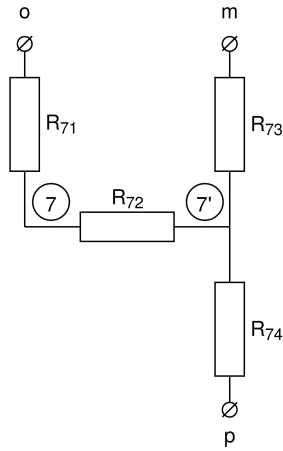
$$R_{62} = \frac{-\tau_p}{b_{rs} 4\pi k_a l_s (r_o^2 - r_i^2)} \left[r_o^2 + r_i^2 - \frac{4r_o^2 r_i^2 \ln\left(\frac{r_o}{r_i}\right)}{r_o^2 - r_i^2} \right]$$

$$R_{63} = \frac{\tau_p}{b_{rs} 2\pi k_a l_s} \left[1 - \frac{2r_i^2 \ln\left(\frac{r_o}{r_i}\right)}{r_o^2 - r_i^2} \right]$$

$$R_{64} = \frac{b_{rs} \pi (r_o^2 - r_i^2)}{\tau_p k_a l_s (r_o - r_i)^2 Q_s^2}$$

$$R_{65} = \frac{\tau_p}{b_{rs} 2\pi k_a l_s} \left[\frac{2r_o^2 \ln\left(\frac{r_o}{r_i}\right)}{r_o^2 - r_i^2} - 1 \right]$$

C.1.7 Rotor Yoke



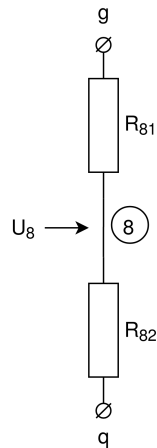
o: to ambient (axial)
 m: to magnets and rotor slots
 p: to ambient (radial)

FIGURE C.7: Node 7: rotor yoke

$$R_{71} = \frac{l_s}{6\pi k_{la}(r_o^2 - r_i^2)} \quad R_{72} = \frac{-1}{4\pi k_{lr} l_s (r_o^2 - r_i^2)} \left[r_o^2 + r_i^2 - \frac{4r_o^2 r_i^2 \ln\left(\frac{r_o}{r_i}\right)}{r_o^2 - r_i^2} \right]$$

$$R_{73} = \frac{1}{2\pi k_{lr} l_s} \left[1 - \frac{2r_i^2 \ln\left(\frac{r_o}{r_i}\right)}{r_o^2 - r_i^2} \right] \quad R_{74} = \frac{1}{2\pi k_{lr} l_s} \left[\frac{2r_o^2 \ln\left(\frac{r_o}{r_i}\right)}{r_o^2 - r_i^2} - 1 \right]$$

C.1.8 End Windings

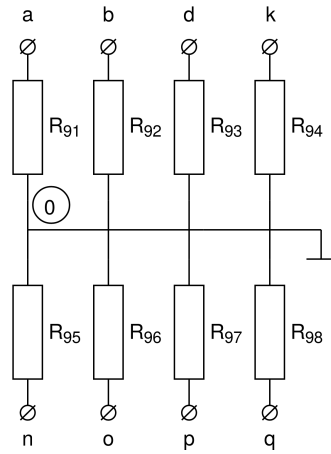


g: to stator windings
 m: to ambients

FIGURE C.8: Node 8: end windings

$$R_{81} = \frac{\pi l_{end}}{6k_{cu} A_{cu} Q_s} \quad R_{82} = \frac{1}{\pi k_v l_{end} F Q_s}$$

C.1.9 Convection to Ambient



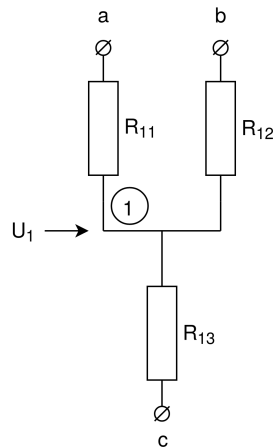
- a: to stator yoke (axial)
- b: to stator yoke (radial)
- d: to stator teeth
- k: to permanent magnets
- n: to rotor slots
- o: to rotor yoke (axial)
- p: to rotor yoke (radial)
- q: to end windings

FIGURE C.9: Node 0: Convection to ambient

$$\begin{aligned}
 R_{91} &= \frac{1}{h_{end}A_{sy(ax)}} & R_{92} &= \frac{1}{h_aA_{sy(rad)}} & R_{93} &= \frac{1}{h_{end}A_{st(ax)}} & R_{94} &= \frac{1}{h_{end}A_{pm(ax)}} \\
 R_{95} &= \frac{1}{h_{end}A_{rs(ax)}} & R_{96} &= \frac{1}{h_{end}A_{ry(ax)}} & R_{97} &= \frac{1}{h_aA_{ry(rad)}} & R_{98} &= \frac{1}{h_{end}A_{end}}
 \end{aligned}$$

C.2 Air-Cored Generator

C.2.1 Stator Windings



- a: to epoxy teeth
- b: to end windings
- c: to epoxy layer

FIGURE C.10: Node 1: stator windings

$$\begin{aligned}
 R_{11} &= \frac{b_s}{2k_vFl_s h_s Q_s} & R_{12} &= \frac{l_s}{2k_{cu}b_s h_s Q_s} & R_{13} &= \frac{h_s}{2k_vFl_s b_s Q_s}
 \end{aligned}$$

C.2.2 Epoxy teeth

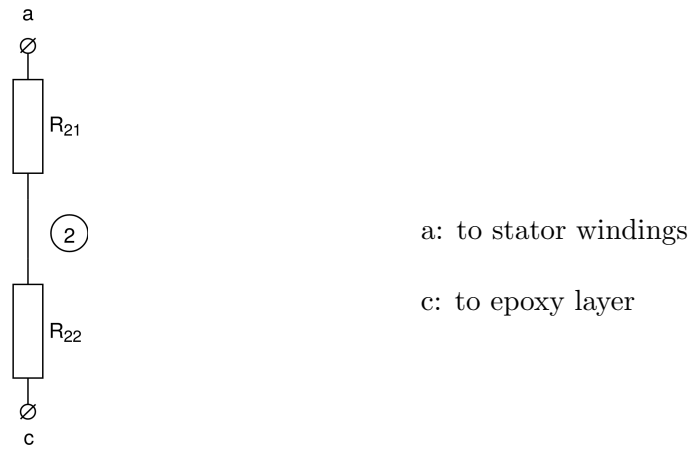


FIGURE C.11: Node 2: epoxy teeth

$$R_{21} = \frac{b_{ep}}{2k_{ep}l_s h_s Q_s} \qquad R_{22} = \frac{h_s}{2k_{ep}l_s b_{ep} Q_s}$$

C.2.3 Epoxy Layer

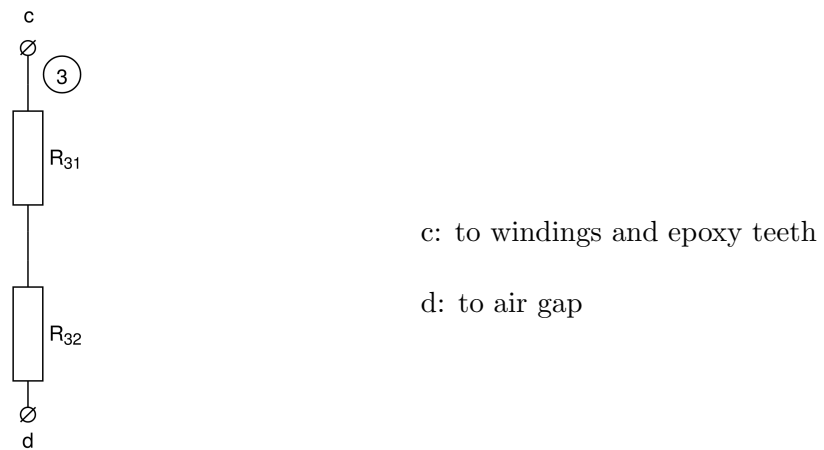
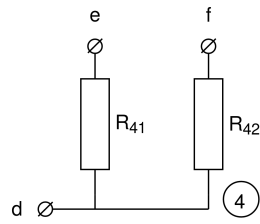


FIGURE C.12: Node 3: epoxy layer

$$R_{31} = \frac{h_{ep}}{k_{ep}\pi(r_o^2 - r_i^2)} \qquad R_{32} = \frac{1}{h_{rs}A_s}$$

C.2.4 Air Gap



e: to permanent magnets

f: to rotor disk

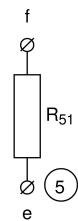
d: to epoxy layer

FIGURE C.13: Node 4: air gap

$$R_{41} = \frac{1}{h_{rs}A_m}$$

$$R_{42} = \frac{1}{h_{rs}(A_s - A_m)}$$

C.2.5 Permanent Magnets



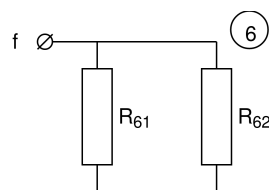
e: to air gap

f: to rotor disk

FIGURE C.14: Node 5: permanent magnets

$$R_{51} = \frac{h_m}{k_m A_m}$$

C.2.6 Rotor Disk



f: to magnets and airgap

FIGURE C.15: Node 6: rotor disk

$$R_{61} = \frac{1}{h_b A_{rb}}$$

$$R_{62} = \frac{1}{h_p A_{rp}}$$

C.2.7 End Windings

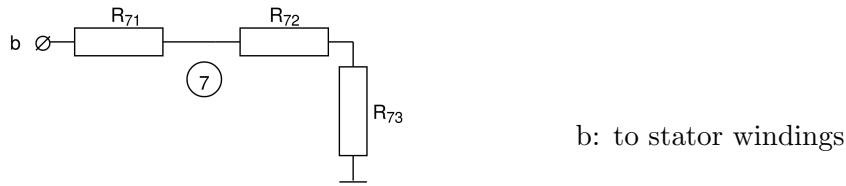


FIGURE C.16: Node 7: end windings

$$R_{71} = \frac{l_{end}}{6k_{cu}A_c u Q_s} \quad R_{72} = \frac{1}{\pi k_v l_{end} F Q_s} \quad R_{73} = \frac{1}{h_{end} A_{end}}$$

C.3 Thermal Resistances

Iron-cored generator

Symbol	Value	Description
R_{11}	0.0650	conduction from stator yoke to axial edge
R_{12}	-0.0068	inner conduction resistance stator yoke
R_{13}	0.0239	conduction from stator yoke to radial edge
R_{14}	0.0285	conduction from stator yoke to teeth and windings
R_{21}	0.9224	conduction from stator teeth to axial edge
R_{22}	-0.0047	inner conduction resistance stator teeth
R_{23}	0.0137	conduction from stator teeth to radial edge
R_{24}	0.0033	conduction from stator teeth to windings
R_{25}	0.0143	conduction from stator teeth to air gap
R_{31}	0.0468	conduction from windings to stator teeth
R_{32}	0.0937	conduction from windings to stator yoke
R_{33}	0.0006	conduction from windings to end windings
R_{34}	0.0935	conduction from windings to air gap
R_{41}	0.8345	convection from air gap to stator teeth
R_{42}	0.6293	convection from air gap to windings
R_{43}	0.8722	convection from air gap to permanent magnets
R_{44}	0.6120	convection from air gap to rotor slots
R_{51}	0.1379	conduction from permanent magnets to axial edge
R_{52}	-0.0048	inner conduction resistance permanent magnets
R_{53}	0.0143	conduction from permanent magnets to air gap
R_{54}	0.2848	conduction from permanent magnets to rotor slots
R_{55}	0.0154	conduction from permanent magnets to rotor yoke
R_{61}	36.08	conduction from rotor slots to axial edge

R_{62}	-1.2556	inner conduction resistance rotor slots
R_{63}	3.742	conduction from rotor slots to air gap
R_{64}	151.3	conduction from rotor slots to permanent magnets
R_{65}	3.791	conduction from rotor slots to rotor yoke
R_{71}	0.0978	conduction from rotor yoke to axial edge
R_{72}	-0.0130	inner conduction resistance rotor yoke
R_{73}	0.0344	conduction from rotor yoke to radial edge
R_{74}	0.0451	conduction from rotor yoke to magnets and rotor slots
R_{81}	0.0015	conduction from end-winding to winding
R_{82}	0.0413	conduction from center of end-winding to edge
R_{91}	0.0512	convection from stator yoke axial to ambient
R_{92}	0.6346	convection from stator yoke radial to ambient
R_{93}	0.7266	convection from stator teeth to ambient
R_{94}	2.6272	convection from permanent magnets to ambient
R_{95}	1.8436	convection from rotor slots to ambient
R_{96}	0.0771	convection from rotor yoke axial to ambient
R_{97}	1.3549	convection from rotor yoke radial to ambient
R_{98}	4.2961	convection from end windings to ambient

Air-cored generator

Symbol	Value	Description
R_{11}	0.9949	conduction from winding to epoxy teeth
R_{12}	0.0199	conduction from winding to end winding
R_{13}	0.0162	conduction from winding to epoxy layer
R_{21}	0.7440	conduction from epoxy teeth to winding
R_{22}	0.2294	conduction from epoxy teeth to epoxy layer
R_{31}	0.0086	conduction from epoxy layer to epoxy teeth and windings
R_{32}	0.2863	convection from epoxy layer to air gap
R_{41}	0.7119	convection from air gap to permanent magnets
R_{42}	0.4789	convection from air gap to rotor disk
R_{51}	0.0049	conduction from permanent magnets to rotor disk
R_{61}	0.0873	convection from back of rotor disk to ambient
R_{62}	0.3147	convection from edge of rotor disk to ambient
R_{71}	0.1193	conduction from end-winding to winding
R_{72}	0.0045	conduction from center of end-winding to edge
R_{73}	0.1205	convection from end-winding to ambient

TABLE C.1: Thermal resistances